# A GEOMETRIC-SENSITIVITY-DIFFERENCE ALGORITHM FOR FLUORESCENCE DIFFUSED OPTICAL TOMOGRAPHY RECONSTRUCTION

By

KRISHNA TEJA TOKALA

Bachelor of Engineering in Electronics and Communication
Vellore Institute of Technology
Vellore, Tamil Nadu
India
2012

Submitted to the Faculty of the
Graduate College of the
Oklahoma State University
in partial fulfillment of
the requirements for
The Degree of
MASTER OF SCIENCE
December, 2013

A GEOMETRIC-SENSITIVITY-DIFFERENCE ALGORITHM FOR FLUORESCENCE DIFFUSED OPTICAL TOMOGRAPHY RECONSTRUCTION

Thesis Approved:

Dr. Daqing Piao

Thesis Adviser

Dr. James West

Dr. Charles F. Bunting

# ACKNOWLEDGEMENTS

I would first want to extend my gratitude and thanks to my advisor Dr. Daqing Piao for helping me and being a very enthusiastic mentor. Without his support and guidance this work would not have been possible. I thank him for recognizing the talent in me and guiding me in the correct path and providing me the opportunity of research assistant under him in his Optical Imaging Laboratory.

This work is dedicated to my parents who are great role model in life. They taught me how to take up challenges and move forward to achieve my goals. Their unconditional love and support help me go through my highs and lows.

I thank my friend Nithya Koka for supporting me at every step of my life.

I am very thankful to Dr. James West who has helped me during the course of Antenna Theory which was a course which not only helped me with the subject but also follow the system of study here in the USA.

I would also like to thank my lab mates of Optical Imaging Laboratory for all the help they have done for completing this work.

Name: KRISHNA TEJA TOKALA

Date of Degree: DECEMBER, 2013

Title of Study: A GEOMETRIC-SENSITIVITY-DIFFERENCE ALGORITHM FOR FLUORESCENCE DIFFUSED OPTICAL TOMOGRAPHY RECONSTRUCTION

Major Field: ELECTRICAL ENGINEERING

Abstract:

Fluorescence Diffused Optical Tomography is an emerging non-invasive imaging technique. Here we have introduced an alternative approach for Fluorescence Diffuse Optical Tomography which optimizes the data model fit based on pairing of the source and detector such that one source is shared by two detectors or one detector is shared by two sources, which in comparison to the conventional data model fit which does not use any kind of pairing. This new reconstruction algorithm is called Geometric Sensitivity Difference (GSD) method which effectively reduces the variation of reconstruction sensitivity with respect to imaging depth. Here the GSD method for source sharing detector pairs is demonstrated using simulated continuous-wave measurements in an outer circular-array imaging geometry, of which the native sensitivity varies strongly with respect to the depth. The results of the GSD method are compared to that of two methods: one is the conventional baseline method which utilizes the native sensitivity and the second method is depth compensation algorithm (DCA) which employs active depth adaptive scheme which counteracts the dependence of reconstruction sensitivity with respect to imaging depth.

TABLE OF CONTENTS

Chapter Page

LIST OF FIGURES

Figure Page

# CHAPTER I

## INTRODUCTION

Prostate is the main part of the man's reproductive system. It is a walnut sized structure which holds the seminal fluid. It is located behind the pelvis under the urinary bladder. The prostate mainly consists of three lobes: a center lobe and two side lobes. This gland which is a very important part of the man's reproductive system is affected by cancer for many American men after the age of 40.[4] Prostate cancer is the 2$^{nd}$ most commonly diagnosed cancer and the 2nd leading cause of cancer deaths in American men.[3]

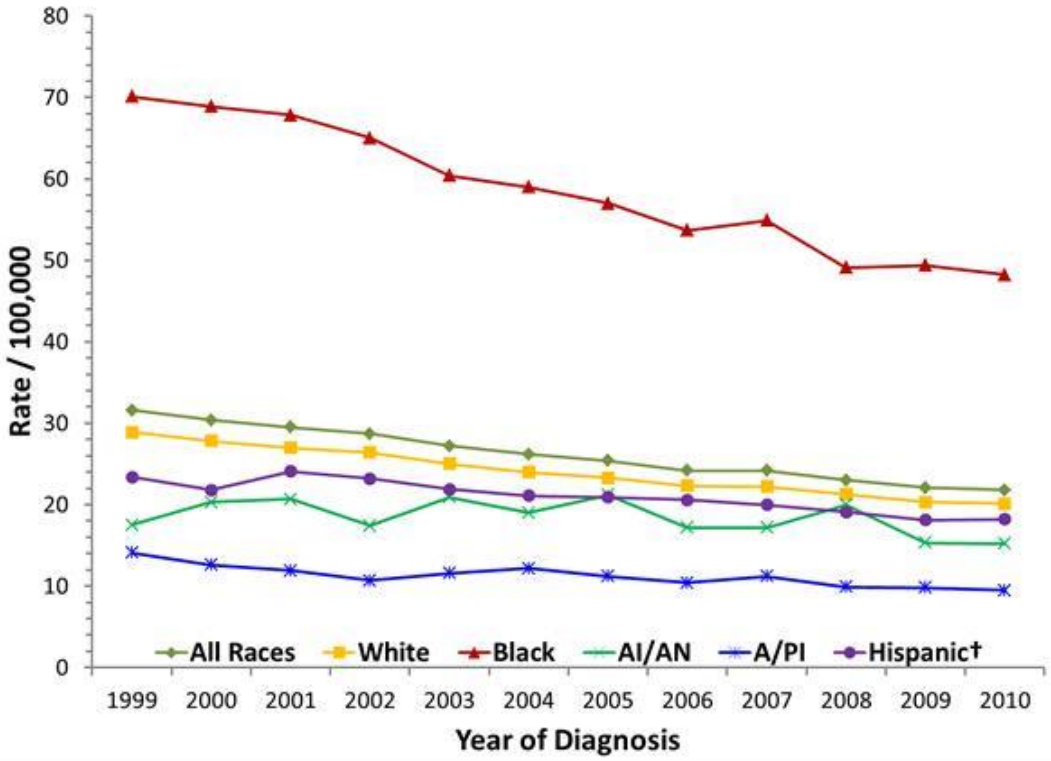


Figure 1. U.S Prostate cancer indices for different races.[2]

The prostate cancer occurs when cells in the prostate gland grow out of control. So detecting the prostate cancer at early stages would help in increasing the survival rate of the patient.

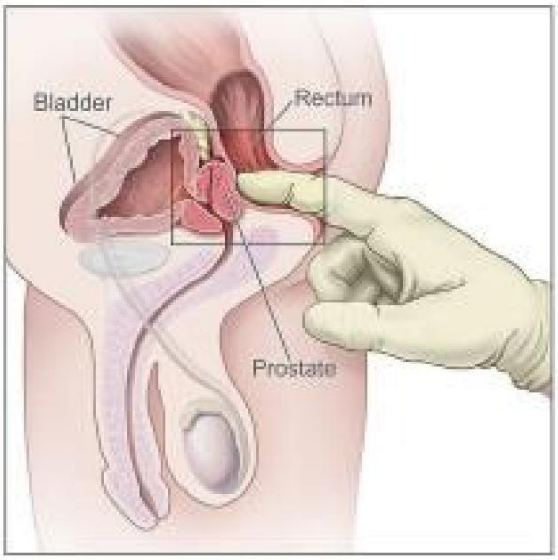


Figure 2. Digital Rectal Exam, In this the doctor/nurse uses their finger to feel the prostate through their rectum. This is done to feel the hard spots [5]

There are usually no early symptoms for prostate cancer patients, although some men might have urinary symptoms and discomfort. So there is a need for a good diagnosis technique for the treatment.

Prostate cancer screening is recommended by use of digital rectal examination (DRE), measurement of serum prostate-specific antigen (PSA), and a combination of these tests.[5] The introduction of PSA screening test has resulted in substantially increased detection of organ-confined prostate cancer or considerable stage migration. However, PSA is not a specific indicator of prostate malignancy and post-treatment tumor recurrence, except after radical prostatectomy. Only a clearly increased serum PSA value (>20 ng/ml) indicates the presence of a prostate carcinoma at a very high probability. [6] In the gray zone between 4 and 10 ng/ml the tissue marker PSA is frequently influenced by benign alterations, so that it is not possible—on the basis of the PSA value alone—to differentiate between benign and malignant cases. DRE can often distinguish between prostate cancer and non-cancerous conditions. DRE may also detect

prostate cancers having normal PSA levels. However, palpation during a DRE is subjective, insensitive, and more than half of all prostate cancers detected today are not palpable.[7-8] The onset of the prostate cancer is confined with biopsy which is the golden standard used in present clinical diagnosis of prostate cancer. Biopsy is generally done when the Digital Rectal Exam and the PCA blood Test are abnormal. To perform this biopsy the doctors need a reliable imaging technique so as to remove the malign tissue part of the prostate for examination. Usually, TRUS guided biopsy is done to help in locating the malign prostate for examination.

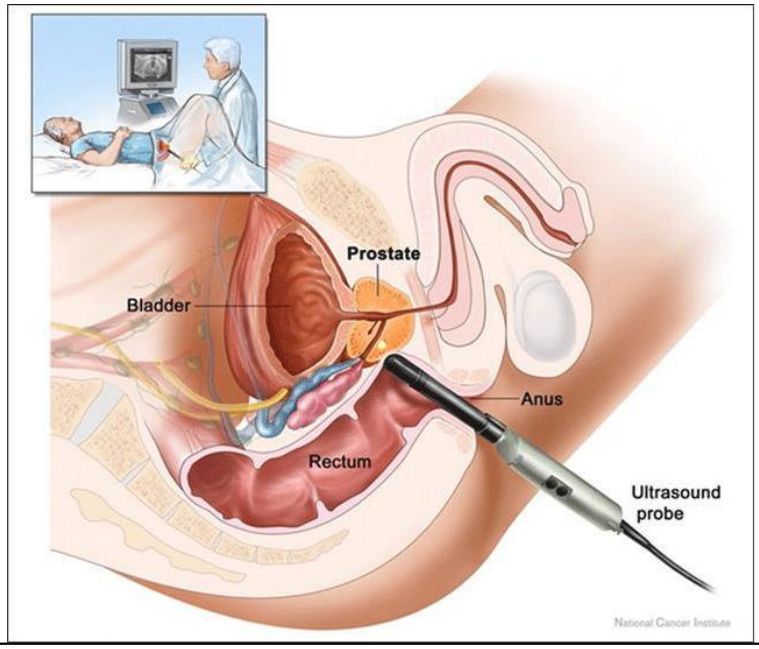


Figure 3. TRUS guided biopsy of human prostate [9]

Prostate cancer may be identified on TRUS as a hypo-echoic lesion. However, at most 60% cancers appear hypo-echoic on TRUS while most of the remaining cancers appear iso-echoic with respect to the surrounding parenchyma.[9] There can be hypo-echoic, cancer-suspicious areas that may be histologically either benign or malignant. TRUS can display the needle trajectory accurately, but it does not differentiate a tumor reliably from normal tissues. The need for many

biopsy-cores for systematic, yet random, tissue sampling of the prostate may be alleviated if the acoustic contrast that TRUS relies on can be augmented with functional or "surrogate" markers of the prostate tumor.[9] The augment of a functional contrast may lead to sampling of the most suspicious lesions. Augmenting TRUS may also desire that such a functional imaging modality be non-invasive and non-ionizing as is TRUS. Optical tomography based on near-infrared (NIR) light could emerge as one such modality.

### 1.1 NIR Optical Tomography

Biological tissue is highly scattering at near-infrared (NIR) wavelengths (600-1000nm),[10] and it can be observed from Fig.4 [10] that in the range of 700-900nm, the absorption of water is much lower than that of oxygenated hemoglobin and deoxygenated hemoglobin. Both features ensure considerable penetration depths and possibility of the measuring tissue oxygen saturation level with near-infrared light. With such theoretical basis and assuming homogeneity in biological tissue, near-infrared optical spectroscopy has been developed to monitor the hemoglobin concentration and oxygen saturation in human tissue with a single source-detector pair.[11] Subsequently, it is demonstrated that with multiple measurements, the heterogeneities of the hemoglobin concentration and oxygen saturation level can actually be resolved, which extends the spectroscopy system to a tomography system as known as Diffused optical tomography (DOT). [13]

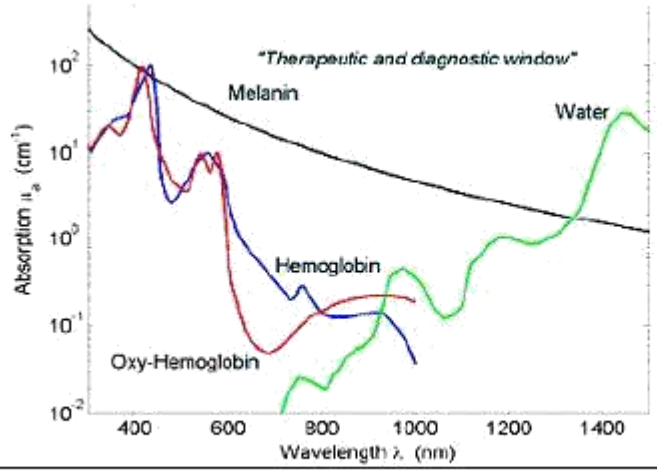


Figure 4. Tissue Optical Window

This method was implemented on imaging of breast, [13] prostate tumors [16] and the analysis of premature infant brain activities [15] and for the imaging of small animals by functional variation of the biological tissue. However the scattering dominates the photon propagation inside the tissue for the NIR tomography so we have a relatively poor spatial resolution.

The instrumentation design of NIR tomography system is determined by the system measurement type and light delivery/collection approaches which are described in brief below.[17,18,19,25]

1. Continuous Wave: Here we use a continuous wavelength light is used in the probing technique in this type of instrumentation. It is used just to measure the attenuation of light through the tissue. This type of instrumentation is relatively very inexpensive and portable. The drawbacks of this type of instrumentation include the difficulty to account for the coupling loses in independently differentiating the effects of absorption and scattering.
2. Time Domain: In this type of instrumentation utilizes pulsed laser sources to transmit light. The Temporal Point Spread Function (TPSF), is measured at the detectors, which is used to determine the time of flight of the photons emitted into the tissue. This can be

related to the absolute scattering and absorption coefficients of the tissue. The drawback of this system is that it is relatively expensive and the system is quite complex as Time Counting Single Photon Counting (TCPSC) systems and pulsed laser diodes require temperature and current controls.

3. Frequency Domain: In this type of instrumentation the light is modulated in the range of 50-500 MHz to produce an intensity modulated, or a frequency domain (FD), light signal. The attenuation of this modulated amplitude and phase shift are measured at the detector. These instruments are relatively cheap and are as robust as the time domain instrumentations in acquiring data when the measurements are taken over a large range of frequencies.

The comparison of the time domain and frequency domain is given in Ref.25.

### 1.2 Zinc as a cancer biomarker for prostate cancer

Besides all the computational and instrumentation improvements on the diffused optical tomography; the implementation of this NIR DOT enhanced with fluorescence emitting material provides an ultimate optical contrast enhancement.

The optical contrast and localization can be substantially increased by the administration of fluorescence emitting agent, which can be followed by trans-rectal imaging, allowing oncologists or urologists seeing the position and extent of the adenocarcinomas of the prostate,[48] and both diagnosis and the planning of surgery could be dramatically improved over the present methods. Zinc is actually well established as a metabolic biomarker for prostate cancer, with changes of at least an order of magnitude in the marker concentration accompanying adenocarcinoma of the prostate. The prostate gland secretes about 10 mM of zinc into prostatic fluid, which is the second-highest concentration found in nature. The zinc secretion of the epithelial cells is biologically analogous to zinc secretion by neurons, salivary cells [58] and breast epithelial cells

[59], with similar transporters sequestering the zinc in the secretory granules. The biological function of the zinc secreted by the prostate epithelial cells is, in short, controlling the time-release of the spermatozoa from the coagulum, in vivo. It is also known that a 10-fold molar excess of citrate is co-secreted with the zinc, thus keeping the zinc in solution as Zn3Citrate2.[72]

The fact that zinc sequestering and secretion are suppressed in adenocarcinomas was first suggested in 1952 and has been consistently documented in many studies since then. It is important to note that the average level of zinc in prostate fluid is reduced by 5- to 10-fold in cancer [72]. Zinc functions as a specific bio-marker to the prostate cancer.[74]

### 1.3 Fluorescence

The feasibility of such approach requires the specificity of the fluorescence agent to either the background tissue or the anomaly target. In this study, fluorescence optical tomography for prostate cancer detection is proposed based on a zinc- specific flurorophor under development of a bio-tech company NeuroBio Tex Inc. in Galveston, TX. One feature distinguishes the zinc-specific fluorophor from the previous investigated ones is that instead of producing fluorophor uptake within the malignant tissue, it concentrates in the benign tissue region. [70-72] Therefore, the imaging scenario will be imaging a dark target within a bright ambience, which will be subjective to significant noise level in the measurement.

By implementing trans-rectal NIR imaging of prostate cancer biomarker such as the zinc using fluorescence tomography (FDOT) measurement, the detection can be made much more specific. There are few of the fluorescent zinc indicator systems excitable in the infrared, except by multi-photon excitation. NeuroBioTex has demonstrated zinc determination using carbonic anhydrase (CA)-based system using infrared two-photon excitation, but the millimeter penetration depth of two-photon excitation (due to pulse spreading, not absorption) as well as the poor transmission of the visible fluorescence will be insufficient for the centimeter-range thickness of the prostate. [73]

In our study we have considered using FDOT in steady state conditions to recover the optical properties of the tissue.

### 1.4 Fluorescence Diffused Optical Tomography

Fluorescent Diffused Optical Tomography is an emerging imaging technique that can spatially resolve both the fluorophore concentration and the lifetime parameters.

For the feasibility of use of this FDOT the functional and structural prior information should be given so as to resolve the above mentioned parameters highly accurately. The functional prior information includes the absorption and scattering mapping of the investigated tissue at the excitation and emission wavelength. The structural prior information includes the boundary of small inclusions or different regions in the background. [20]

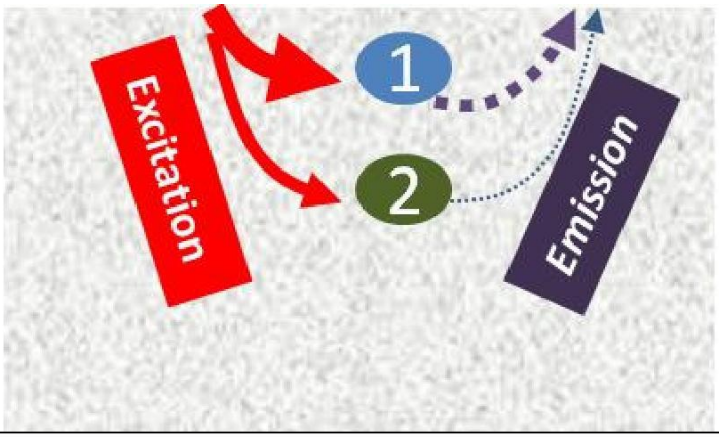


Figure 5. The principle of fluorescence diffused optical tomography is shown here. The fDOT has two wavelengths to be considered, one being the excitation and the other being emission. As the result we have coupled equations where the targets named 1 and 2 emit out wavelengths depending on their absorption and fluorescence contrast. [20]

Recently, fluorescence probe techniques have been extended to in-vivo imaging areas. Monitoring of drug biological processes have been very helpful in determining the disease at very early stages.

Although the reconstruction of the FDOT is very similar to Diffused optical tomography (DOT),

but the light modeling inside the tissue is quite complex for FDOT. First the propagation of the excitation light should be modeled from the boundary to the fluorophore which is located deep inside the tissue. Then the propagation of the emitted light should be modeled from the fluorophore to the detectors which are at the boundary of the tissue.[22] Accordingly the absorption and scattering parameters at the excitation and emission wavelengths should be obtained prior to reconstruction of fluorescence parameters.

### 1.5 Challenges in Fluorescence Diffused Optical Tomography

It is very important to realize that the FDOT image recovery problem is inherently prone to a few challenges and is very difficult to solve from a mathematical or a computational point of view. This is primarily because the propagation of light in the tissue is non-linear, leading to the following challenges; [75]

Non-linear: Linear changes in optical properties do not give linear changes in detected signal.

Ill-posed: Smaller changes in the detected signal gives rise to large changes in the estimated optical properties, making the problem prone to large estimation error due to noise and other external conditions.

Under-determined: The number of independent equations that we have are lesser than the number of properties to be determined. It is also called ill-determined.

Depth dependent-sensitivity: The objects at a deeper depth from the boundary of the optodes is reconstructed at approximately the same depth of the maximum sensitivity profile.

These features imply that there is no unique solution for a given set of independent equations/for the given detected signal. Due to this non-uniqueness problem we need to constrain the solution space, by using regularization. Regularization involves formulating the inversion as an iterative model-based linear algebra problem. This kind of formulation poses constrains on the real time computational methods

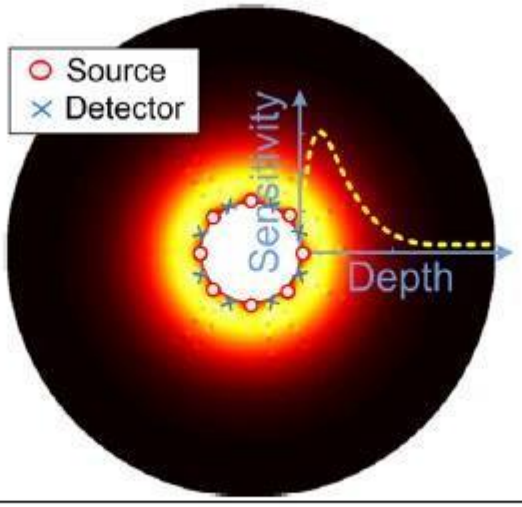


Figure 6. Endoscopic Imaging Geometry for prostate cancer imaging. The dotted yellow line shows how the sensitivity varies with respect to the imaging depth.

Here in our study we consider an endoscopic imaging geometry for prostate cancer as shown in Figure 6. The spatially non-uniformity sensitivity is unfavorable due to the resulted non-uniformity in contrast, resolution, and particularly the biased localization of the anomaly at the position of the local sensitivity peak.

### 1.6 Motivation and Objective

Diffuse optical tomography enhanced with fluorescence-contrast is an active area of optically rendered imaging that has the potential to achieve molecular sensitivity and high specificity in

diagnosis. A surface measurement of the fluorescence photon to resolve the distribution of endogenous or extraneous fluorophore usually involves an array of illumination and detection points at the medium-applicator interface. The medium-applicator interfaces relevant to reflective-mode diffuse fluorescence measurements and the photon propagation in any of these geometries could be modeled by diffusion as long as the measurement distance exceeds several times of the transport scattering scale. Fluorescence Diffuse optical tomography (fDOT) is inherently prone to spatially-dependent sensitivity, due to scattering-dominated photon propagation in biological tissue. The spatial dependence of fDOT sensitivity is also specific to the geometry of the interface between the medium and the array of optodes. The optode-array of fDOT usually has one- or two-dimensional symmetry that gives rise to a sensitivity distribution that is mostly uniform along the direction of the symmetry except at locations close to the optodes. For example, the spatial sensitivity of a circular array that has evenly distributed optodes along the circumference is azimuthally invariant and the spatial sensitivity of a near-planar array whereupon the optodes are orderly distributed changes insignificantly over the lateral dimension of the array. However, at the directions orthogonal to the symmetry of the optode configuration, specifically along the depth into the medium, the spatial sensitivity varies, generally with a pronounced peak in the proximity of the medium-array interface.

Such variation of the sensitivity causes depth-dependent reconstruction of the contrast and resolution. More severely, it may cause objects of different depths to be recovered at approximately the same depth, the position at which the radial profile of the sensitivity peaks. The depth-dependence of the sensitivity is thus a common issue to be negotiated in many fDOT applications, including those to brain, to breast using planar remission geometry and to prostate via endo-rectal probing for either sagittal or axial imaging, etc. Among these fDOT applications, the endo-rectal axial-imaging geometry is subjected to arguably the strongest variation of the sensitivity with respect to imaging depth, due to the rapid reduction of photon fluence versus the

source-detector distance when compared with the geometries involving a planar interface or a curved interface that encloses the medium. As will be shown, localizing the depth of an object of interest in such circular-array outward-imaging geometry is challenging.

So there is a need of using a robust method to localize the target in this endo-rectal probing for fDOT to image the prostate in its early stages. This is where the GSD method [1] is implemented which uses the paired measurements to localize the object location at the correct depth making the geometry less sensitive with respect to the depth variation from the optodes array to reconstruct the anomaly at correct depth so as to localize the malign region for biopsy.

### 1.7 Organizing of Thesis

The rest of the thesis is arranged as follows. Chapter 2 The forward and inverse reconstruction algorithms of NIRFAST software are discussed in this section. It presents the analytical formations of GSD method as it applies to fDOT image reconstruction in the context of Levenberg–Marquardt (LM) minimization using paired continuous-wave (CW) measurements from source-sharing source-detector-pairs. Chapter 2 also describes two reconstruction approaches against which the GSD method will be evaluated: one is a conventional or baseline method that applies a spatially invariant regulation in the LM minimization; and the other is a reference-compensation approach [32-33] which is similar in methodology to the DCA method but is more robust than the original DCA method for the circular-array outward-imaging geometry of this study. Chapter 3 deals with the circular-array axial outward-imaging geometry to be studied, of which the native sensitivity with respect to imaging depth varies significantly more than those of planar or circular-array inward-imaging geometries. The simulation results in Chapter 3 demonstrate that the GSD method generally outperforms the baseline and depth-compensation methods, in terms of localizing the depth of single object, resolving two azimuthally separated objects, and estimating the optical property of single object or azimuthally

separated dual objects in the circular-array outward-imaging geometry. As all three methods involve a step-specific regularization scheme in the iterations, the same step-specific regularization factor optimal to the reference-compensation method is applied to the base-line reconstruction and the GSD based reconstruction. An outperformance of the GSD method over the base-line method is unsurprising at all, because the effective sensitivity profile of the former method is much more uniform with respect to the imaging depth than that of the latter method. The outperformance of the GSD method over the depth-compensation method, shall relate to the pairing measurements by the former method versus the un-paired measurements by the latter method. Chapter 3 also deals with using the GSD applied to negative contrast target which is analogous to reconstructing a negative contrast fluorescence target in the case of prostate using a zinc biomarker.

# CHAPTER II

## COMPUTATIONAL MODELLING

The propagation of photon flux can be analytically modeled by the diffusion approximation of the radiative transfer equation. For imaging geometry, human tissue can be modeled as either infinite (optode inserted into the tissue) or semi-infinite (surface detection).

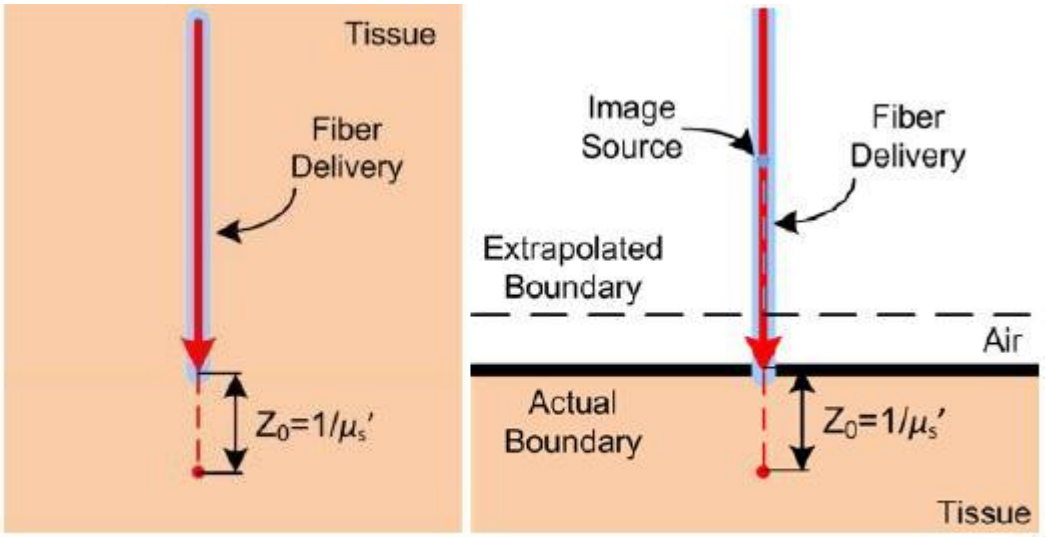


Figure 7. The Figure on the right shows an infinite imaging geometry. The figure on the left shows the semi-infinite imaging geometry.

The modeling of NIR tomography consists of two parts: 1) a forward model, which represents the light interaction to the medium being imaged; and 2) an inverse model, which is solved for the optical properties of the imaged medium. [30] For the forward model of NIR tomography, explicit analytical solution of the light propagation can be solved. For a semi-infinite medium, by applying mirror method with the precondition that photon density is zero at the extrapolated boundary, the solution for the photon propagation in infinite medium is derived. However, for

more complicated tomography cases, which reconstructs the spatially varied of optical property distribution, numerical methods such as finite element method and finite difference method are used. As to inverse model, NIR tomography reconstruction iteratively fits the forward model to the actual measurements.

## 2.1 Forward Model

In the frequency domain of photon propagation in a turbid medium it is known that the propagation of both excitation and fluorescent emission light in tissues or multiple scattering media can be described by the following coupled diffusion equations.

$$\nabla.[D_x(\vec{r})\nabla\varphi_x(\vec{r})] - [\mu_{ax}(\vec{r})]\varphi_x(\vec{r}) = -S(\vec{r}) \quad (1)$$

$$\nabla.[D_m(\vec{r})\nabla\varphi_m(\vec{r})] - [\mu_{am}(\vec{r})]\varphi_m(\vec{r}) = -\eta(\vec{r})\mu_a^{fl}\varphi_x(\vec{r}) \quad (2)$$

Where $\varphi_{x,m}$ is the photon density for excitation ($x$) and emission of the fluorescent light ($m$). $D_{x,m}$ is the diffusion coefficient, $\mu_{a(x,m)}$ is the absorption coefficient from both the non-fluorescing chromopheres and the fluorescent dye, $\mu_a^{fl}$ is the absorption co-efficient for the excitation light due to the contribution from the fluorescent dye, ω is the modulation frequency and $c$ is the velocity of light in the medium, and η is the fluorescent quantum yield and τ is the life time of the fluorescent dye.

The diffusion coefficient is written as :

$$D_{x,m}(\vec{r}) = 1/3[\mu_{a(x,m)}(\vec{r}) + \mu'_{s(x,m)}(\vec{r})] \quad (3)$$

Hence, for the known optical properties Eqs. (1) and (2) reduces to standard boundary value problems for spatially varying photon densities of excitation and emission light subject to the Robin-type boundary conditions (III – BC) which is considered to give most accurate results. On applying the III-BC to the medium applicator interface we get,

$$-D_{x,m}(\vec{r})\nabla\varphi_{x,m}.\hat{n} = \alpha\varphi_{x,m} \quad (4)$$

Where $\hat{n}$ is the unit vector pointing outwards normal to the interface and α is a co-efficient determined by the reflective index mismatch across the boundary. By the phasor notation $\varphi_{x,m} = Ie^{j\theta}$ so this can be implemented in specifies the algorithm as,

$$\log\left[\varphi_{x,m}(\vec{r})\right] = \log\left(I_{x,m}\right) + j\theta \quad (5)$$

So as to get a better scaled inverse problem for the reconstruction. The purpose of fDOT is to recover all the distributions including $D_{x,m}, \mu_{a(x,m)}, \tau \; and \; \eta$. Here we are mainly concerned about the reconstruction of $\eta\mu_a^{fl}$.

### 2.2 Inverse Reconstruction Model

An individual source-detector pair, $\langle S_i, D_j \rangle$, consisting of a source *i* and a detector *j* which are used in the data model fit (χ) of the conventional objective function of fDOT inverse problem is thereby:

$$||\Psi^{ex}||^2 = \left|\left|\left[\varphi_{\{\langle S_i,D_j\rangle\}}{}^{ex}\right]_M - \left[\varphi_{\{\langle S_i,D_j\rangle\}}{}^{ex}(\chi)\right]_C\right|\right|^2 \quad (6a)$$

$$||\Psi^{em}||^2 = \left|\left|\left[\varphi_{\{\langle S_i,D_j\rangle\}}{}^{em}\right]_M - \left[\varphi_{\{\langle S_i,D_j\rangle\}}{}^{em}(\chi)\right]_C\right|\right|^2 \quad (6b)$$

Where χ refers to optical property of interest. *m* and *c* represent 'measurement' and 'calculation' respectively.

This function is done at every iteration until the error is minimized. This equation after Taylor series expansion around the μ values and ignoring the higher order terms:

$$[\varphi^{ex}(\chi_n)]_C \approx [\varphi^{ex}(\chi_{n-1})]_C + J^{ex}\delta\chi \quad (7a)$$

$$[\varphi^{em}(\chi_n)]_C \approx [\varphi^{em}(\chi_{n-1})]_C + J^{em}\delta\chi \quad (7b)$$

Where subscripts *n* and *n-1* are the iteration numbers and $\delta\mu_n$ is the difference between the present value and the previous iteration value. The *J* in eq. (7a,b) is the Jacobian, or called the sensitivity matrix, which is the first order derivative of the measurement quantities with respect to the optical properties. Here *J* corresponds to the excitation and emission matrices ($J^{ex,em}$) which have been discussed in the later part of the section.

Therefore, the update of the optical properties at nth iteration is given by:

$$\delta\chi_n = (J^T J)^{-1} J^T \Psi_{n-1} \quad (8)$$

In order to facilitate a good reconstruction a Levenberg-Marquardt scheme implements a diagonal regularization factor λ in the form of

$$\delta\chi_n = (J^T J + \lambda I)^{-1} J^T \Psi_{n-1} \quad (9)$$

The value of λ value is used as 100 and an empirical damping factor of 1.78 is used.

We have N as the total number of spatial elements for which the updating of the optical properties is reconstructed. "NoS" as the number of source channels, and "NoD" as the number of detector channels. As we have mentioned above about the *J* for both excitation and emission we have the complete coupled Jacobian matrices which are given by:

$$J^{ex}_{[NoD*NoS*2]\times[N*2]} = \begin{bmatrix} [\frac{\partial \log(I^{ex})}{\partial \mu_a^{ex}}]_{[NoD*NoS]\times N} & [\frac{\partial \log(I^{ex})}{\partial D^{ex}}]_{[NoD*Nos]\times N} \\ [\frac{\partial \theta}{\partial \mu_a^{ex}}]_{[NoD*Nos]\times N} & [\frac{\partial \theta}{\partial D^{ex}}]_{[Nod*Nos]\times N} \end{bmatrix} \quad (10a)$$

$$J^{em}_{[NoD*NoS*3]\times[N*3]} =$$

$$\begin{bmatrix} [\frac{\partial \log(I^{em})}{\partial \mu_a^{em}}]_{[NoD*NoS]\times N} & [\frac{\partial \log(I^{em})}{\partial D^{em}}]_{[NoD*NoS]\times N} & [\frac{\partial \log(I^{em})}{\partial \eta\mu_a^{fl}}]_{[NoD*Nos]\times N} \\ [\frac{\partial \theta}{\partial \mu_a^{em}}]_{[NoD*NoS]\times N} & [\frac{\partial \theta}{\partial D^{em}}]_{[NoD*NoS]\times N} & [\frac{\partial \theta}{\partial \eta\mu_a^{fl}}]_{[NoD*NoS]\times N} \end{bmatrix} \quad (10b)$$

Here the analytical formulation of the GSD method discussed for the CW case can be straightforwardly extended to recovering all the properties $\mu_{a(x,m)}, D_{x,m}$ , $\eta \; and \; \tau$. The extentsions involve either doubling the columns or doubling the number of both columns and rows.

So in the remaining analytics, let us consider $J^{ex,em} = [\frac{\partial \log(I^{ex,em})}{\partial \chi}]$ where log(I) can be replaced by ψ and χ is the change in the parameters in the above jacobians i.e $\eta\mu_a^{fl}$. In the later part of the analytics we will also specify the NoD=16 and Nos=16, to the outward circular geometry used in the simulation studies. With these changes the Jacobian matrices to be written as a single matrix for avoiding confusion becomes:

$$J^{ex,em<>} = [\frac{\partial \psi}{\partial \chi^{<>}}]_{256\times N} = [\, J^1 \, J^2 \, J^3 \, \dots \dots \, J^N], \qquad (11a)$$

Where $J^{ex,em^{<>}}$ and $\chi^{<>}$, <> = {1:N}, are respectively, the sub-matrix of $J$ and χ associated with the "<>th" element. $J^{<>}$ has a dimension of 256×1 and is shown as:

$$J^{ex,em<>} =$$

$$[\, J^{ex,em<>}_{\langle S_1,D_1\rangle} \dots J^{ex,em<>}_{\langle S_{16},D_{16}\rangle} \, , J^{ex,em<>}_{\langle S_2,D_1\rangle} \dots J^{ex,em<>}_{\langle S_2,D_{16}\rangle} \dots \dots J^{ex,em<>}_{\langle S_{16},D_1\rangle} \dots J^{ex,em<>}_{\langle S_{16},D_{16}\rangle} \qquad (11b)$$

This shows the sensitivity of the measurement by the source-detector pair with respect to the "<>th" special element.

### 2.3 Continuous wave steady-state measurements

The continuous steady-state measurement uses the DC light source to directly measure the attenuation of the light power. Although the frequency domain and the time domain approaches provide more optical information than the CW approach, researchers are more inclined to CW due to the relative simplicity, cost effectiveness and high SNR.

Here in our analytics too we have considered CW steady state measurements where the lifetime of the fluorophore is considered zero.

The previously demonstrated methods, that make the reconstruction less sensitive to the object depth, may be different in terms of how the native sensitivity profile was compensated or counteracted. As in some the actions were imposed indirectly by the regularization but in others were applied directly to the sensitivity function; however, all these methods were similar, in terms of fitting the calculated data to the ***individual measurements taken by individual source-detector-pairs***. This study introduces an alternative method of optimizing the data-model fit, which is to fit the calculated data to the ***paired measurements taken by two source-detector-pairs that share either the source or the detector.*** An intuitive explanation of this method is that, although the sensitivity of one pair of source-detector with respect to an object could vary significantly over the depth of the object, the relative response between two pairs of source-detector that share one optode could vary substantially less over the depth with respect to the same object, and hypothetically the image reconstruction based on this relative or paired response could be more robust in localizing the object than that based on the response of individual pairs of source-detector. The relative response between two optode-sharing source-detector-pairs to a given medium heterogeneity is related to the positioning (i.e. geometric) difference of the heterogeneity with respect to the two source-detector-pairs, therefore, the reconstruction scheme that takes advantage of such relative or paired response is called a geometric-sensitivity difference (GSD) based reconstruction. The objective of this study is to demonstrate that the GSD method effectively evens the reconstruction updating sensitivity with respect to imaging depth and consequently improves fDOT depth-localization. The GSD differs from previously investigated depth-compensation reconstruction method in that it does not involve depth-adapted or to-be-optimized parameters in order to reduce the variation of the reconstruction sensitivity with respect to imaging depth.

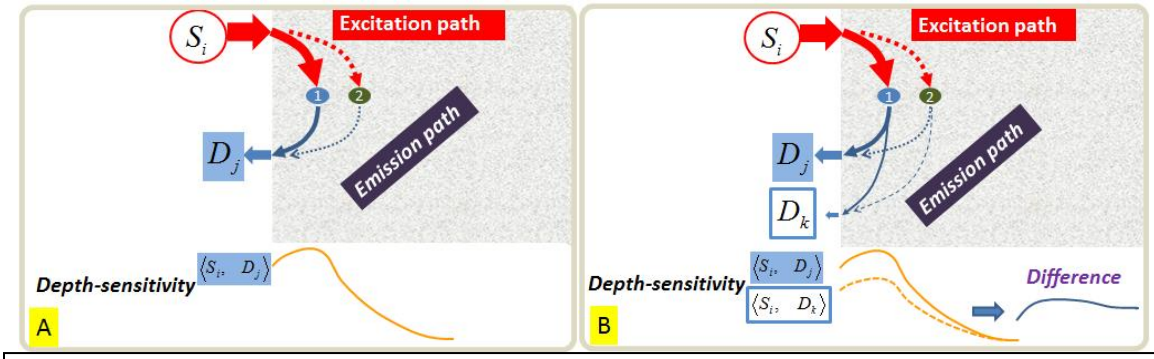


Figure8. Illustration of the fDOT reconstruction approaches which utilize the paired measurements from two source-sharing source-detector-pairs. The solid curve represents the native sensitivity profile of $\langle S_i, D_j \rangle$, the dashed curve represents native sensitivity of $\langle S_i, D_k \rangle$. (a) The signal response of a source and a detector; (b) the relative differences between the signal responses of $\langle S_i, D_j \rangle$ and $\langle S_i, D_k \rangle$ to the same object located at different depths are different, yet the difference between the sensitivity profiles is less depth dependent.

### 2.4 Geometric Sensitivity Difference Reconstruction using source detector pairing

We analyze the forward pairing between the two source detector pairs i.e $\langle S_i, D_j \rangle$ *and* $\langle S_i, D_m \rangle$ with j < m. The relative sensitivity of the measurements with respect to the <>th element is

$$\frac{\partial\left[\psi_{\langle S_i,D_j\rangle} - \psi_{\langle S_i,D_m\rangle}\right]}{\partial \chi^{<>}} = \frac{\partial \psi_{\langle S_i,D_j\rangle}}{\partial \chi^{<>}} - \frac{\partial \psi_{\langle S_i,D_m\rangle}}{\partial \chi^{<>}} \tag{12}$$

$$= J^{<>}_{\langle S_i,D_j\rangle} - J^{<>}_{\langle S_i,D_m\rangle} = \tilde{J}^{<>}_{\langle S_i,D_j,D_m\rangle}\,.$$

This illustrates the complete forward pairing of the Source-Detector pairs, for example the forward solving solution with respect to $\langle S_1, D_1 \rangle$ is given by $\tilde{J}^{<>}_{\langle S_i,D_j,D_m\rangle}$ with $i$ = 1, $j$ =1, $m$={2:16}, which is of the form,

$$\begin{matrix}\tilde{J}^{<>}_{\langle S_1,D_1,D_2\rangle}\\ \tilde{J}^{<>}_{\langle S_1,D_1,D_3\rangle}\\ \tilde{J}^{<>}_{\langle S_1,D_1,D_4\rangle}\\ \tilde{J}^{<>}_{\langle S_1,D_1,D_5\rangle}\\ \tilde{J}^{<>}_{\langle S_1,D_1,D_6\rangle}\\ \tilde{J}^{<>}_{\langle S_1,D_1,D_7\rangle}\\ \tilde{J}^{<>}_{\langle S_1,D_1,D_8\rangle}\\ \tilde{J}^{<>}_{\langle S_1,D_1,D_9\rangle}\\ \tilde{J}^{<>}_{\langle S_1,D_1,D_{10}\rangle}\\ \tilde{J}^{<>}_{\langle S_1,D_1,D_{11}\rangle}\\ \tilde{J}^{<>}_{\langle S_1,D_1,D_{12}\rangle}\\ \tilde{J}^{<>}_{\langle S_1,D_1,D_{13}\rangle}\\ \tilde{J}^{<>}_{\langle S_1,D_1,D_{14}\rangle}\\ \tilde{J}^{<>}_{\langle S_1,D_1,D_{15}\rangle}\\ \tilde{J}^{<>}_{\langle S_1,D_1,D_{16}\rangle}\end{matrix} = \begin{bmatrix} 1 & -1 & 0 & 0 & 0 & 0 & 0 & 0 & 0 & 0 & 0 & 0 & 0 & 0 & 0 & 0\\ 1 & 0 & -1 & 0 & 0 & 0 & 0 & 0 & 0 & 0 & 0 & 0 & 0 & 0 & 0 & 0\\ 1 & 0 & 0 & -1 & 0 & 0 & 0 & 0 & 0 & 0 & 0 & 0 & 0 & 0 & 0 & 0\\ 1 & 0 & 0 & 0 & -1 & 0 & 0 & 0 & 0 & 0 & 0 & 0 & 0 & 0 & 0 & 0\\ 1 & 0 & 0 & 0 & 0 & -1 & 0 & 0 & 0 & 0 & 0 & 0 & 0 & 0 & 0 & 0\\ 1 & 0 & 0 & 0 & 0 & 0 & -1 & 0 & 0 & 0 & 0 & 0 & 0 & 0 & 0 & 0\\ 1 & 0 & 0 & 0 & 0 & 0 & 0 & -1 & 0 & 0 & 0 & 0 & 0 & 0 & 0 & 0\\ 1 & 0 & 0 & 0 & 0 & 0 & 0 & 0 & -1 & 0 & 0 & 0 & 0 & 0 & 0 & 0\\ 1 & 0 & 0 & 0 & 0 & 0 & 0 & 0 & 0 & -1 & 0 & 0 & 0 & 0 & 0 & 0\\ 1 & 0 & 0 & 0 & 0 & 0 & 0 & 0 & 0 & 0 & -1 & 0 & 0 & 0 & 0 & 0\\ 1 & 0 & 0 & 0 & 0 & 0 & 0 & 0 & 0 & 0 & 0 & -1 & 0 & 0 & 0 & 0\\ 1 & 0 & 0 & 0 & 0 & 0 & 0 & 0 & 0 & 0 & 0 & 0 & -1 & 0 & 0 & 0\\ 1 & 0 & 0 & 0 & 0 & 0 & 0 & 0 & 0 & 0 & 0 & 0 & 0 & -1 & 0 & 0\\ 1 & 0 & 0 & 0 & 0 & 0 & 0 & 0 & 0 & 0 & 0 & 0 & 0 & 0 & -1 & 0\\ 1 & 0 & 0 & 0 & 0 & 0 & 0 & 0 & 0 & 0 & 0 & 0 & 0 & 0 & 0 & -1 \end{bmatrix} \begin{matrix} J^{<>}_{\langle S_1,D_1\rangle}\\ J^{<>}_{\langle S_1,D_2\rangle}\\ J^{<>}_{\langle S_1,D_3\rangle}\\ J^{<>}_{\langle S_1,D_4\rangle}\\ J^{<>}_{\langle S_1,D_5\rangle}\\ J^{<>}_{\langle S_1,D_6\rangle}\\ J^{<>}_{\langle S_1,D_7\rangle}\\ J^{<>}_{\langle S_1,D_8\rangle}\\ J^{<>}_{\langle S_1,D_9\rangle}\\ J^{<>}_{\langle S_1,D_{10}\rangle}\\ J^{<>}_{\langle S_1,D_{11}\rangle}\\ J^{<>}_{\langle S_1,D_{12}\rangle}\\ J^{<>}_{\langle S_1,D_{13}\rangle}\\ J^{<>}_{\langle S_1,D_{14}\rangle}\\ J^{<>}_{\langle S_1,D_{15}\rangle}\\ J^{<>}_{\langle S_1,D_{16}\rangle}\end{matrix} \quad (13a)$$

$$[\tilde{J}^{<>}_{\langle S_1,D_1,D_{2:16}\rangle} = \left[Diff^{<>}_{\langle S_1,D_1,D_{2:16}\rangle}\right]_{15\times 16} \times [J^{<>}_{\langle S_1,D_1\rangle} J^{<>}_{\langle S_1,D_2\rangle} \dots\dots J^{<>}_{\langle S_1,D_{16}\rangle}]^T \quad (13b)$$

Here the [diff] matrix which is used is called the GSD matrix operator and it helps in forward pairing differentiation of the native sensitivity values. The [Diff] matrix in eq. (16b) is of dimension 15×16 whereas the complete forward solver of the GSD operator for $\langle S_1, D_j\rangle$ is $j$ = {2:16}, will generate a [Diff] matrix that has a dimension of (16-$j$) × 16.

This method is applied for all the N spatial elements, a matrix transformation of the native sensitivity J by a complete and non-redundant forward pairing GSD operator [Diff] follows as

$$\tilde{J} = [Diff]J \quad (14)$$

Where the dimension of $\tilde{J}$ is [(NoD-1)*NoD/2*NoS] × 1 × N, that of [Diff] is [(NoD-1)*NoD/2*NoS] × [NoS*NoD] ×N and that of $J$ is given by [NoS*NoD] × 1 × N. The matrix multiplication is done for the first two dimensions of the three matrices. The third

dimension N indicates that the matrix multiplication has been done N times and hence, the *J* is represented in such a way.

By using the GSD operator in eq. (17), the conventional objective function eq. (6) for reconstruction changes to

$$||\Psi||^2 = \left|\left|[Diff]\left[\varphi_{\{\langle S_i,D_j\rangle\}}{}^{em}\right]_m - [Diff]\left[\varphi_{\{\langle S_i,D_j\rangle\}}{}^{em}(\chi)\right]_c\right|\right|^2 \quad (15)$$

$$= \left|\left|\left[\varphi_{\{\langle S_i,D_j\rangle\}}{}^{em}\right]_m - \left[\varphi_{\{\langle S_i,D_j\rangle\}}{}^{em}(\chi)\right]_c\right|\right|^T [Diff]^T[Diff] \left|\left|\left[\varphi_{\{\langle S_i,D_j\rangle\}}{}^{em}\right]_m - \left[\varphi_{\{\langle S_i,D_j\rangle\}}{}^{em}(\chi)\right]_c\right|\right|$$

Here both Ψ and $\varphi$ are now column vectors that have [NoS*NoD*(NoD-1)/2] rows. Accordingly, eq. (11) and eq. (12) transforms to:

$$\delta\chi_n = (\tilde{J}^T\tilde{J})^{-1}\tilde{J}^T\Psi_{n-1} \quad (16)$$

$$\delta\chi_n = (\tilde{J}^T\tilde{J} + \lambda I)^{-1}.\tilde{J}^T\Psi_{n-1} \quad (17)$$

These equations are valid for both excitation and emission of the reconstruction process.

### 2.5 Choice of reconstruction method to which GSD is compared

Comparing the GSD method to the baseline method is straight forward as we know that the FDOT of the baseline method does not use the depth compensation scheme. So this GSD method is compared to that of the DCA method which involves the depth compensation scheme which involves the operation on the Jacobian matrix of the reconstruction process.

### 2.5.1 Choice of reconstruction method to which GSD is compared

DCA study is applied to this circular-outward imaging geometry whose sensitivity is much greater than that compared to the geometries that were previously considered. This method modifies the sensitivity matrix by weighting scheme of $J_R = M^{\gamma} J$ to achieve the updated function for retrieving the optical properties as follows:

$$\delta\chi_n = ([J_R]^T J_R + \lambda I)^{-1} . [J_R]^T \Psi_{n-1} \quad (18)$$

The weighting implementation in DCA in implementing $J_R$is M = {diag[MSV($J_l$), MSV($J_{l-1}$),…, MSV($J_2$), MSV($J_1$)]}, where MSV stands for maximum singular value of the sensitivity terms in $J_l$. The subscripts {1, 2,….$l$} denote the number of the layer over a depth and $\gamma$ is the power factor. The number of layers and the power factor are the two parameters that have to be optimized in the above equation. In the previous study the DCA method was tested on this outward circular imaging geometry and the effect of this method to effectively compensate for the depth was too strong compared to that demonstrated for the planar geometry. So an enhanced method of the DCA was used called the reference compensation algorithm which is identical to Eq. (18) except that,$J_R = M^{SVR} J$, where $M^{SVR}$is the a sensitive compensation matrix that is exponentially regulated according to the radial depth of the spatial element. For the studied circular-array of outward imaging geometry with inner radius of 10mm the diagonal elements of $M^{SVR}$are calculated for each of the N spatial elements with respect to their distance (ρ) from the center of the geometry as

$$M^{SVR}(i,j) = \begin{cases} 500 exp^{\frac{\rho_i - 10}{R-10}} & \text{if i = j i. e diagonal element} \\ 0 & \text{else} \end{cases} \quad (19)$$

### 2.6 Effective sensitivity distribution and regularization of parameters

The effective sensitivity distribution over the entire imaging geometry can be evaluated by summing the sensitivity terms corresponding to the same spatial element <> and associated with the source detector pairs, i.e.,$\sum[J^{<>}_{\{<S_i,D_j>\}}]$for the baseline method [Fig. 5(a)], $\sum[J^{<>}_{\{R_{<S_i,D_j>}\}}]$ for the DCA method [Fig. 5(b)], and $\sum[\tilde{J}^{<>}_{\{<S_i,D_j,D_m>\}}]$ for the GSD method [Fig. 5(c)]. The depth sensitivity along the radial direction is plotted as shown in Fig. 5(d). The GSD method involves a slight rearrangement of the terms of sensitivity matrix. For example if the signs of all $\tilde{J}^{<>}_{\{<S_i,D_j,D_m>\}}$ terms that satisfy m-j>8 are reversed, the rows containing paired blocks with the **bold *italic*** such as "***1***" and"***-1***" will incur a sign change to the paired blocks, denoted by "***1*** → ***(-1)***" and "***(-1)*** → ***1***", i.e the reversing of the order of $J^{<>}_{\langle S_i,D_j\rangle}$ and $J^{<>}_{\langle S_i,D_m\rangle}$ in $\tilde{J}^{<>}_{\{<S_i,D_j,D_m>\}}$. This is because of the crossing of the measurements of the source detector pairs as shown in Ref.1.

This adjusted $\tilde{J}^{<>}_{\{<S_i,D_j,D_m>\}}$ is implemented in our simulations and is compared with the effective distribution profiles of the native sensitivity J, and the depth compensation applied sensitivity$J_R$, along a marked depth direction. It can be appreciated that the effective sensitivity profile of the GSD is nearly depth invariant and insignificant comparing to the other two methods. The DCA out performs the base-line method as it peaks at a significantly increased depth. The parameters that we have used for the DCA method are explicitly described in Ref (1).

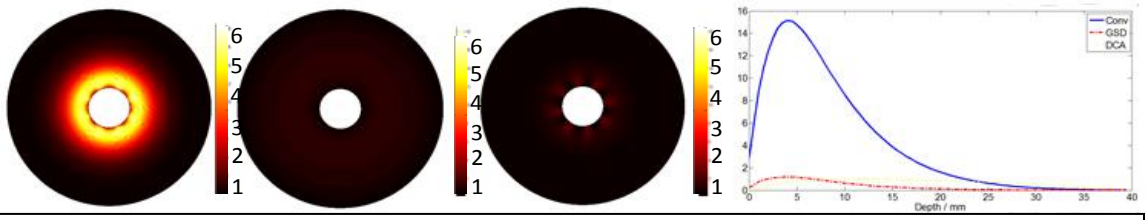


Figure9. Conceptual illustration of the principle of Depth-dependences of the conventional (a), depth compensated algorithm (b) and geometric sensitivity difference (c), respectively. (d) Shows the depth plot of the 3 methods along the yellow dotted line.

# CHAPTER III

## RESULTS AND DISCUSSION

In this simulation study we are using a circular-array outward imaging geometry as is shown in Fig.(number). This imaging geometry has inner radius of 10mm and outer radius of 50mm, with 16 source and 16 detectors. This mesh is generated using finite element method and the parameters of the background and the anomaly are given in table I and II. Here the outer boundary is not a physical boundary as the internal one where the sources and detectors are placed. We make sure the radius of the imaging geometry is sufficiently large such that it does not interfere with the photon fluence rate in the imaging region proximal to the inner boundary. Here we consider only a two-dimensional geometry because we are primarily concerned about the reconstruction of the object in the plane of the optodes. So the 2-D annular imaging domain applying to the geometry of Fig.7 was discretized into a fem mesh with 7664 evenly distributed nodes and 14820 elements. The display of the sensitivity distributions, forward and inverse computations were realized based on NIRFAST for a 16 source detector pairs on the inner boundary for the geometry. The potential of the GSD method is alleviating the sensitivity variation with respect to the imaging depth maybe graphically appreciated by comparing the sensitivity profiles of the neighboring source sharing source detector pairs as shown in Ref.1.

The optical heterogeneities that are employed for the simulation were either a single circle or a two such identical circles which are separated azimuthally. The circles, i.e the anomalies are of 5mm radius and are placed at a distance of 0.5mm, 5mm, and 10mm from the detection array.

The optical properties of the anomaly are listed in Table I and Table II. The contrast of the anomaly is 3 times the background for the positive contrast case and 1/3 times for the negative contrast case. A Gaussian noise of 1% was added to this set of forward computation unless otherwise specified. In the remaining sections the three methods were simulated and the

comparison is shown by placing them side by side. These methods were run explicitly in different scenarios to compare the outcome:

(1) Single anomaly case with positive contrast at 0.5mm, 5mm and 10mm from the optode array.

(2) Single anomaly case with negative contrast at 0.5mm, 5mm and 10mm from the optode array.

(3) Dual anomaly case with positive contrast with a fixed azimuthal separation of $90^o$ and at depths of 0.5mm, 5mm and 10mm from the optode array.

(4) Dual anomaly case with negative contrast with a fixed azimuthal separation of $90^o$ and at depths of 0.5mm, 5mm and 10mm from the optode array.

(5) Dual anomaly case with positive contrast with a fixed depth of 10mm from the optode array and different azimuthal separation of $45^o$, $135^o$, $180^o$.

(6) Dual anomaly case with negative contrast with a fixed depth of 5mm from the optode array and different azimuthal separation of $45^o$, $135^o$, $180^o$.

| Parameter | Tissue property | Anomaly Property |
|---|---|---|
| Dimension | Inner Rad-10mm ; Outer Rad-50mm | Radius-5mm. Placed at 0.5,5,10 deep from the optode array. |
| Absorption Co-eff | Muax – 0.01mm-1;<br>Muam – 0.01mm-1 | Muax - 0.01mm-1<br>Muam – 0.01mm-1 |
| Scattering Co-eff | Musx – 1.00mm-1<br>Musm – 1.10mm-1 | Musx – 1.00mm-1<br>Musm – 1.10mm-1 |
| Refractive Index | 1.33 | 1.33 |
| Fl. Quantum Yield | 0.1 | 0.2 |
| Fl. Absorption | 0.01mm-1 | 0.0150mm-1 |

TABLE II

### 3.1 Positive contrast target with respect to the background

#### 3.1.1 Single Anomaly

A single anomaly has been placed at the depths of 0.5mm, 5mm, and 10mm from the optode array. The properties of the anomaly and the background are described in Table I. This setup simulation was run for the three methods and the radial one dimensional profile was extracted for each depth and compared.

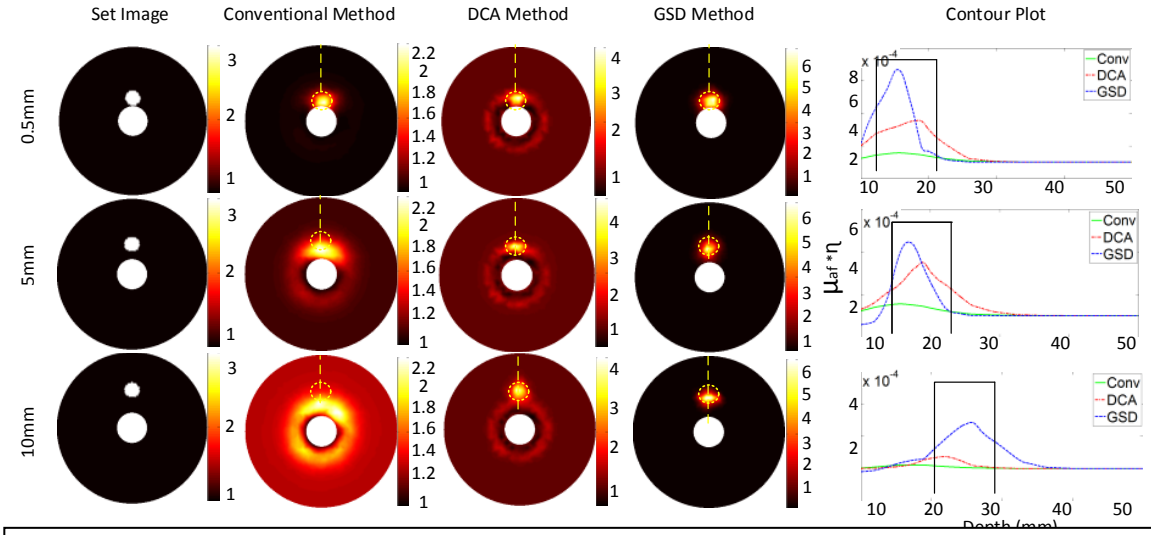


Figure 11.Simulations experiments examining target depth recovery (Unit:$10^{-4}$·$mm^{-1}$). Columns (a) set values; (b) conventional reconstruction; (c) depth compensation reconstruction and (d) GSD reconstruction. Column (e) contour plot along the yellow dotted lines in colume (b)(c)(d).

In the figure 11 (a)-(d) it is observed that by using the baseline method the objects at the three different depths are reconstructed at the same depth close to the optical detection array. The GSD method and the DCA method recover the object at approximately the true depth. The object optical properties were underestimated by all the three methods; however the underestimation was least for GSD method.

#### 3.1.2 Dual Anomaly at different depths

Two anomalies have been placed at the same depths of 0.5mm, 5mm, and 10mm from the optode array with an azimuthal separation of 90°. The properties of the anomalies and the background are

described in Table I. This setup simulation was run for the three methods and the azimuthal one dimensional profile was extracted for each depth and compared.

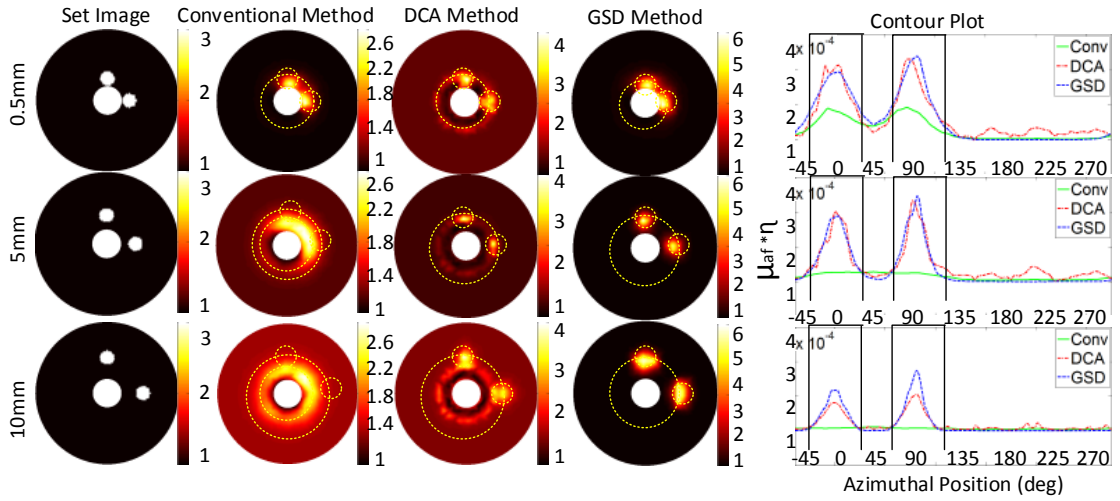


Figure12.Simulations examining target depth recovery(Unit:$10^{-4}mm^{-1}$). Columns (a) set values; (b) conventional reconstruction; (c) depth compensation reconstruction and (d) GSD reconstruction. Column (e) contour plot along the yellow dotted lines in colume (b)(c)(d).

In the figure 12 (a)-(d) it is observed that by using the baseline method the objects at the three different depths are reconstructed at the same depth close to the optical detection array. At a depth of 10mm from the optode array the conventional method is unable to distinguish between the two targets. The GSD method and the DCA method recover the object at approximately the true depth and can differentiate between the two target locations. However the GSD shows a better contrast between the two objects compared to the DCA as the depth increases. The object optical properties were underestimated by all the three methods; however the underestimation was least for GSD method.

### 3.1.3 Dual Anomaly at different azimuthal separation

Two anomalies have been placed at the same depth of 5mm from the optode array with azimuthal separations of 45°, 135°, 180°. The properties of the anomalies and the background are described

in Table I. This setup simulation was run for the three methods and the azimuthal one dimensional profile was extracted for each depth and compared.

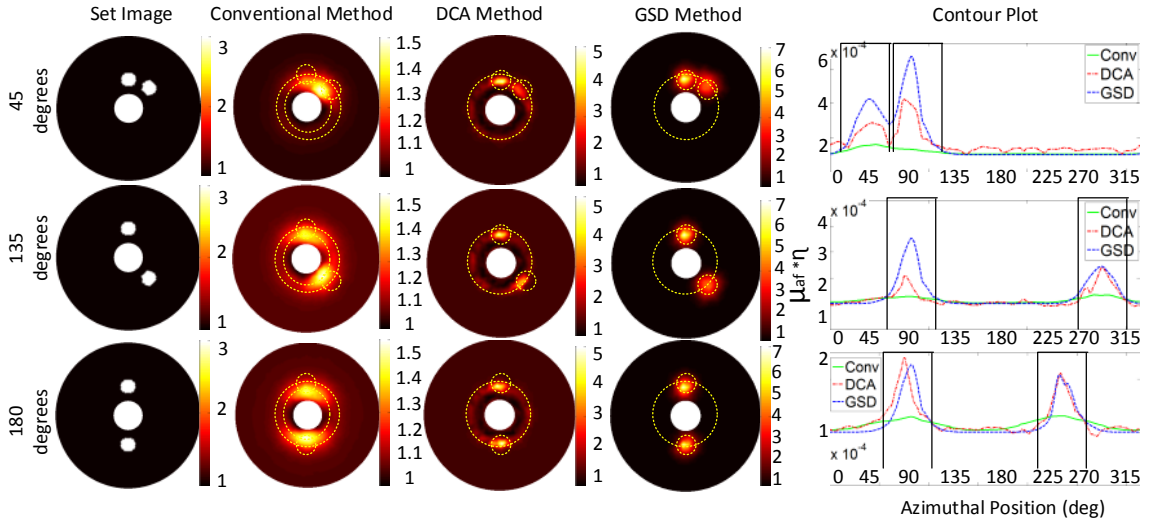


Figure13.Simulations experiments examining target depth recovery (Unit:$10^{-4}mm^{-1}$). Columns (a) set values; (b) conventional reconstruction; (c) depth compensation reconstruction and (d) GSD reconstruction. Column (e) contour plot along the yellow dotted lines in colume (b)(c)(d).

In the figure 13 (a)-(d) it is clearly shown that the GSD can outperform the DCA and the conventional baseline reconstruction. For the reconstructed images at 45 degrees GSD is able to reconstruct and show a clear contrast of the targets as compared to the DCA and the Conventional reconstruction.

### 3.2 Negative contrast target with respect to the background

#### 3.2.1 Single Anomaly

A single anomaly has been placed at the depths of 0.5mm, 5mm, and 10mm from the optode array. The properties of the anomaly and the background are described in Table II. This setup simulation was run for the three methods and the one dimensional profile was extracted for each depth and compared.

| Parameter | Tissue property | Anomaly Property |
|---|---|---|
| Dimension | Inner Rad-10mm ; Outer Rad-50mm | Radius-5mm. Placed at 0.5,5,10 deep from the optode array. |
| Absorption Co-eff | Muax – 0.01mm-1;<br>Muam – 0.01mm-1 | Muax - 0.01mm-1<br>Muam – 0.01mm-1 |
| Scattering Co-eff | Musx – 1.00mm-1<br>Musm – 1.10mm-1 | Musx – 1.00mm-1<br>Musm – 1.10mm-1 |
| Refractive Index | 1.33 | 1.33 |
| Fl. Quantum Yield | 0.1 | 0.05 |
| Fl. Absorption | 0.01mm-1 | 0.0067mm-1 |

TABLE III

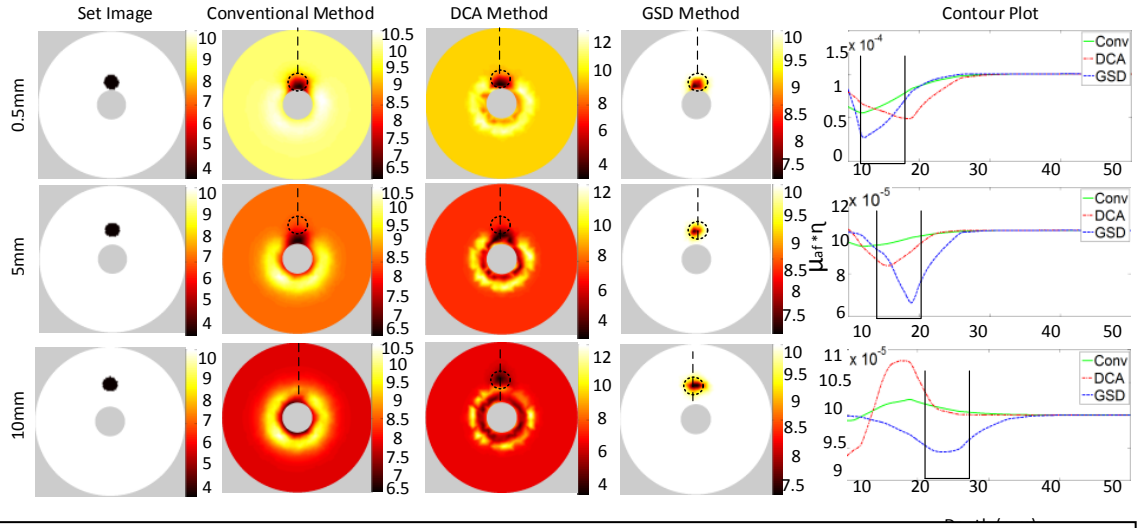


Figure14. Simulations and experiments examining target depth recovery (Unit:$10^{-5}$·$mm^{-1}$). Columns (a) set values; (b) conventional reconstruction; (c) depth compensation reconstruction and (d) GSD reconstruction. Column (e) contour plot along the black dotted lines in colume (b)(c)(d).

In the figure 14 (a)-(d) it is observed that by using the baseline method the objects at the three different depths are reconstructed at the same depth close to the optical detection array. The GSD method and the DCA method recover the object at approximately the true depth. The object

optical properties were underestimated by all the three methods. It can also be confirmed that the negative contrast anomaly is hard to recover as compared to the positive contrast target as the conventional baseline reconstruction method cannot reconstruct the target at a distance of 10mm, whereas in a positive anomaly case it can even though it is at the detector array. Yet GSD helps in locating the target at approximately at the correct depth even though the recovered fluorescent contrast with respect to the background is quite low. When the target depth goes greater than 25mm GSD is also unable to locate the target and all the three methods fail.

### 3.2.2 Dual Anomaly at different depths

Two anomalies have been placed at the same depths of 0.5mm, 5mm, and 10mm from the optode array with an azimuthal separation of 90°. The properties of the anomalies and the background are described in Table II. This setup simulation was run for the three methods and the azimuthal one dimensional profile was extracted for each depth and compared.

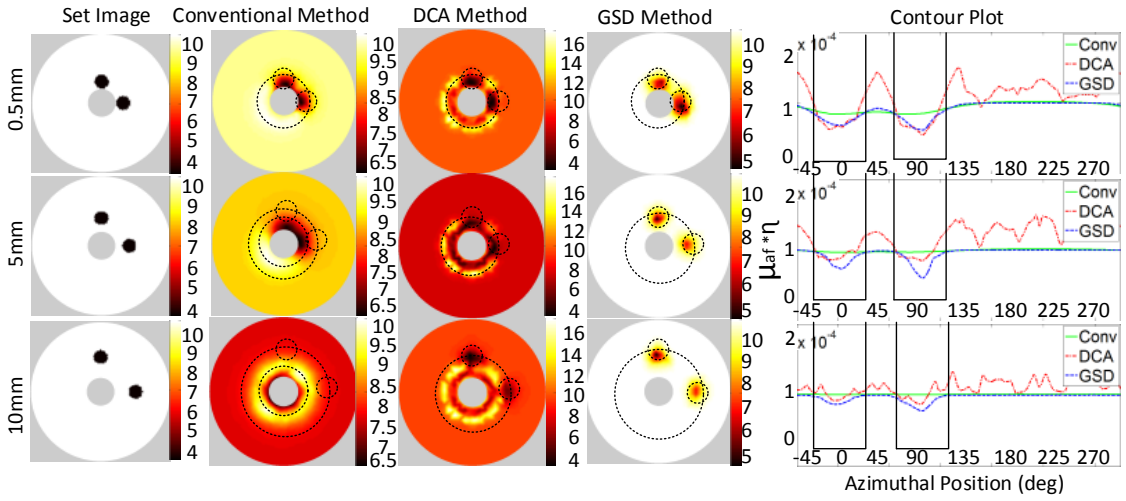


Figure15.Simulations experiments examining target depth recovery (Unit:$10^{-5}$·$mm^{-1}$). Columns (a) set values; (b) conventional reconstruction; (c) depth compensation reconstruction and (d) GSD reconstruction. Column (e) contour plot along the black dotted lines in colume (b)(c)(d).

### 3.2.3 Dual Anomaly at different azimuthal separation

Two anomalies have been placed at the same depth of 5mm from the optode array with azimuthal separations of 45°, 135°, 180°. The properties of the anomalies and the background are described in Table II. This setup simulation was run for the three methods and the azimuthal one dimensional profile was extracted for each depth and compared.

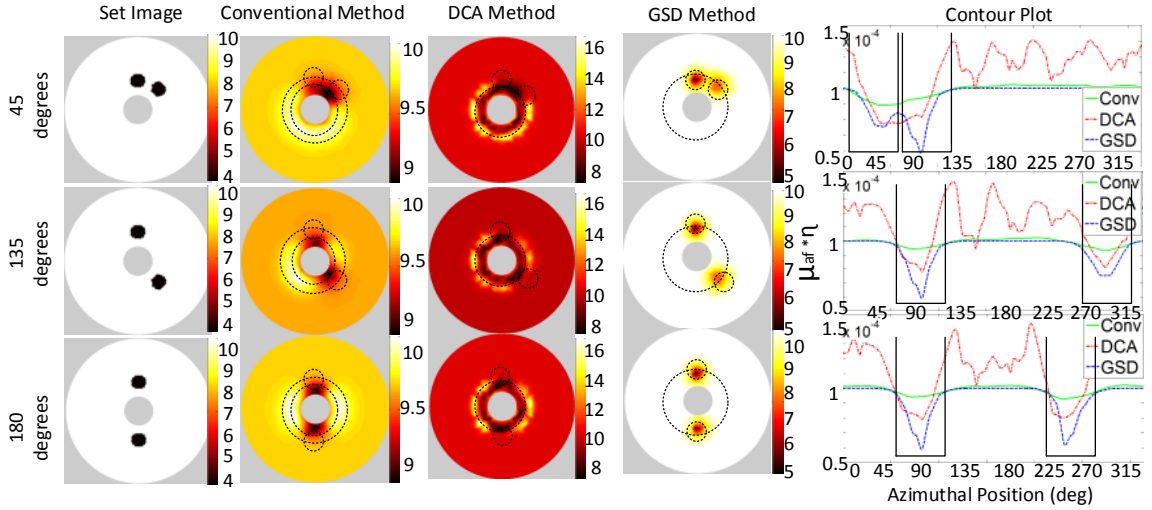


Figure 16. Simulations experiments examining target depth recovery (Unit:$10^{-5}$·$mm^{-1}$). Columns (a) set values; (b) conventional reconstruction; (c) depth compensation reconstruction and (d) GSD reconstruction. Column (e) contour plot along the black dotted lines in colume (b)(c)(d).

In the figure 16 (a)-(d) it is clearly shown that the GSD can outperform the DCA and the conventional baseline reconstruction. For the reconstructed images at 45 degrees GSD is able to reconstruct and show a clear contrast of the targets as compared to the DCA and the Conventional reconstruction.

# CHAPTER IV

# CONCLUSION AND FUTURE WORK

This study demonstrates an alternative approach FDOT image reconstruction by optimizing the data model fit with the individual source-detector measurements. This method which is called the GSD method helps in optimizing the data model fit by taking the advantage of the paired measurements of the source-detector-pairs. It effectively and passively suppresses the spatial variance of the detection sensitivity with respect to depth taking advantage of the relative changes of the measurements of two optode-sharing source-detector pairs. It is demonstrated that this GSD method improves the depth localization for FDOT in an axial outward imaging circular geometry that is considered to have the strong sensitivity variation with respect to imaging depth. Simulated measurements based on CW are used to evaluate the performance of GSD over the other two methods: the conventional algorithm which does not involve any depth adaptation scheme and the depth compensation algorithm which involves the active depth dependent compensation scheme.

The GSD method clearly outperforms the other two methods in terms of localizing the object at correct depth and also resolving them azimuthally correctly and estimating the optical properties for both single object and dual object cases.

The GSD method however is more computational demanding due to the increase in the jacobian matrix and due to more matrix multiplications. The effectiveness of this method is associated with the symmetry of the optode array.

## 6.1 Future work

This methodology was carried out experimentally on DOT and works equally well with FDOT too. This is an in-silico study and should be experimentally validated in the future.

The prostate tissue just like any other epithelial cells have the ability to accumulate high levels of zinc, there has been found to be a decrease in the levels of zinc in the human prostate at the sight of malignancy creating a negative contrast with respect to the background. Fluorescent contrast bio markers which are specific to Zinc can be used in to image prostate cancer at a very early stage and localizing the tumor can be done effectively by this method.

# REFERENCES


1. Guan.Xu; Daqing Piao, 2013 “A geometric-sensitivity-difference based algorithm improves object-depth localization for diffused optical tomography in a circular-array outward imaging geometry. Med. Phy 0094-2405/2013

2. American cancer society: Cancer facts, Atlanta, GA, 2011

3. Siegel R, (2011). "Cancer statistics, 2011: the impact of eliminating socioeconomic and racial disparities on premature cancer deaths." CA Cancer J Clin 61: 212–36. doi:10.3322/caac.20121.PMID 21685461.

4. Baade PD; Youlden DR; Krnjacki LJ (2009 Feb). "International epidemiology of prostate cancer: geographical distribution and secular trends." Molecular nutrition & food research 53 (2): 171–84.PMID 19101947.

5. Moore, K.; Dalley, A. (1999). Clinically Oriented Anatomy. Baltimore, Maryland: Lippincott Williams & Wilkins. ISBN 0-683-06132-1.

6. Y Lin, H Gao, O Nalcioglu and G Gulsen,”Fluorescence diffused optical tomography with functional aprior information: feasibility study. Phys. Med. Biol. **52** (2007) 5569–5585

7. Scott C. Davis, Hamid Dehghani, Jia Wang, Shudong Jiang, Brian W. Pogue and Keith D. Paulsen, “ Image guided diffuse optical tomography implemented in Laplacian-type regularization”. 2 April 2007 / Vol. 15, No. 7 / OPTICS EXPRESS 4068.

8. Y. Paithankar, A. U. Chen, B. W. Pogue, M. S. Patterson, and E. M. Sevick-Muraca, "Imaging of fluorescent yeild and lifetime from multiply scattered light reemitted from random media," Appl. Opt. **36**, 2260-2272 (1997).

9. B. J. Tromberg, A. Cerussi, N. Shah, M. Compton, A. Fedyk, D. Hsiang, J. Butler, and R.Mehta, “Diffuse Optics in Breast Cancer: Detecting Tumors in Pre-Menopausal Women and Monitoring Neoadjuvant Chemotherapy”,Breast Cancer Research **7**, 279–285 (2005).

10. A. P Gibson, J. C. Hebden, and S. R. Arridge, “Recent advances in diffuse optical imaging,” Phys. Med. Biol. **50**, R1–R43 (2005).

11. I. Nissila, J. C. Hebden, D. Jennions, J. Heino, M. Schweiger, K. Kotilahti, T. Noponen, A.Gibson, S. Jarvenpaa, L. Lipiainen, and T. Katila, “Comparison between a time-domain and a frequency-domain system for optical tomography,” J. Biomed. Opt. **11**, 064015:1-18 (2006).

12. S R Arridge, “Optical tomography in medical imaging,” Inv. Problems **15**, R41–R93 (1999).

13. H. B. Jiang, "Frequency-domain fluorescent diffusion tomography: a finite-element-based algorithm and simulations," Appl. Opt. **37**, 5337-5343 (1998).

14. D. J. Hawrysz, and E. M. Sevick-Muraca, "Developments toward diagnostic breast cancer imaging using near infrared optical measurements and fluorescent contrast agents," Neoplasia **2**, 388-417 (2000).

15. A. Godavarty, A. B. Thompson, R. Roy, M. Gurfinkel, M. J. Eppstein, C. Zhang, and E. M. Sevick-Muraca, "Diagnostic imaging of breast cancer using fluorescence-enhanced optical tomography: phantom studies," J.Biomed. Opt. **9**, 488-496 (2004).

16. S. R. Arridge, M. Schweiger, M. Hiraoka and D. T. Delpy, "A finite element approach for modeling photon transport in tissue," Med. Phys. **20**, 299-309 (1993).

17. M. Huang and Q. Zhu, “Dual-mesh optical tomography reconstruction method with a depth correction that uses a priori ultrasound information,” Appl. Opt. **43**(8), 1654–1662 (2004).

18. H. Niu, F. Tian, Z.-J. Lin, and H. Liu, “Development of a compensation algorithm for accurate depth localization in diffuse optical tomography,” Opt. Lett. **35**(3), 429–431 (2010).

19. Xu, D. Piao, C. H. Musgrove, C. F. Bunting, and H. Dehghani, "Trans-rectal ultrasound-coupled near-infrared optical tomography of the prostate, Part I: Simulation," Opt. Express **16**(22), 17484–17504 (2008).

20. Q. Zhao, L. Ji, and T. Jiang, "Improving depth resolution of diffuse optical tomography with a layer-based sigmoid adjustment method," Opt. Express **15**(7), 4018–4029 (2007).

21. S. R. Arridge, "Optical tomography in medical imaging," Inverse Probl.**15**(2), R41–R93 (1999).

22. D. S. Kepshire, S. C. Davis, H. Dehghani, K. D. Paulsen, and B. W. Pogue, "Subsurface diffuse optical tomography can localize absorber and fluorescent objects but recovered image sensitivity is nonlinear with depth," Appl. Opt. **46**(10), 1669–1678 (2007).

23. F. Tian, G. Alexandrakis, and H. Liu, "Optimization of probe geometry for diffuse optical brain imaging based on measurement density and distribution," Appl. Opt. **48**(13), 2496–2504 (2009).

24. B. W. Pogue, T. O. McBride, J. Prewitt, U. L. Österberg, and K. D. Paulsen, "Spatially variant regularization improves diffuse optical tomography," Appl. Opt. **38**(13), 2950–2961 (1999).

25. D. Piao, H. Xie, C. Musgrove, C. F. Bunting, W. Zhang, G. Zhang, E. B. Domnick-Davidsion, K. E. Bartels, G. R. Holyoak, S. N. Vemula- palli, H. Dehghani, and B. W. Pogue, *Near-Infrared Optical Tomography: Endoscopic Imaging Approach*, *Proc. SPIE 6431*, Multimodal Biomedical Imaging II, 643103 (2007).

26. J. P. Culver, A. M. Siegel, J. J. Stott, and D. A. Boas, "Volumetric diffuse optical tomography of brain activity," Opt. Lett. **28**(21), 2061–2063 (2003).

27. Zhang, D. Piao, C. F. Bunting, and B. W. Pogue, "Photon diffusion in a homogeneous medium bounded externally or internally by an infinitely long circular cylindrical applicator. I. Steady-state theory," J. Opt. Soc. Am. A **27**(3), 648–662 (2010).

28. D. W. Marquardt, “An algorithm for least-squares estimation of nonlinear parameters,” J. Soc. Ind. Appl. Math. **11**(2), 431–441 (1963).

29. P. K. Yalavarthy, B. W. Pogue, H. Dehghani, and K. D. Paulsen, “Weight- matrix structured regularization provides optimal generalized least-squares estimate in diffuse optical tomography,” Med. Phys. **34**(6), 2085–2098 (2007).

30. H. Dehghani, M. E. Eames, P. K. Yalavarthy, S. C. Davis, S. Srinivasan, C. M. Carpenter, B. W. Pogue, and K. D. Paulsen, “Near infrared optical tomography using NIRFAST: Algorithm for numerical model and image reconstruction,” Commun Numer. Methods Eng. **25**(6), 711–732 (2009).

31. Corlu, R. Choe, T. Durduran, K. Lee, M. Schweiger, S. R. Arridge, E. M.Hillman, and A. G. Yodh, “Diffuse optical tomography with spectral constraints and wavelength optimization,” Appl. Opt. **44**(11), 2082–2093 (2005).

32. H. Bastian, “On uniqueness in diffuse optical tomography,” Inverse Probl. **25**(5), 055010 (14pp) (2009).

33. Y. Xu, X. Gu, T. Khan, and H. Jiang, “Absorption and scattering images of heterogeneous scattering media can be simultaneously reconstructed by use of dc data,” Appl. Opt. **41**(25), 5427–5437 (2002).

34. G. Xu, D. Piao, C. F. Bunting, and H. Dehghani, “Direct-current-based image reconstruction versus direct-current included or excluded frequency- domain reconstruction in diffuse optical tomography,” Appl. Opt. **49**(16), 3059–3070 (2010).

35. H. Niu, Z.-J. Lin, F. Tian, S. Dhamne, and H. Liu, “Comprehensive inves- tigation of three-dimensional diffuse optical tomography with depth com- pensation algorithm,” J. Biomed. Opt. **15**(4), 046005–046009 (2010).

36. V. Ntziachristos, A. G. Yodh, M. Schnall, and B. Chance, “Concurrent MRI and diffuse optical tomography of breast after indocyanine green enhance- ment,” Proc. Natl. Acad. Sci. U.S.A. **97**(6), 2767–2772 (2000).

37. G. Xu and D. Piao, *Feasibility of Rapid Near-Infrared Diffuse Optical Tomography by Swept-Spectral-Encoded Sequential Light Delivery, Proc. SPIE 7896,* Optical Tomography and Spectroscopy of Tissue IX, 78961W (2011).

38. K. Lange, D. R. Hunter, and Y. Ilsoon, "Optimization transfer using surro-gate objective functions," J. Comput. Graph. Stat. **9**(1), 1–20 (2000).

39. H. Xu, B. W. Pogue, R. Springett, and H. Dehghani, "Spectral derivative based image reconstruction provides inherent insensitivity to coupling and geometric errors," Opt. Lett. **30**(21), 2912–2914 (2005).

40. M. Schweiger, I. Nissilä, D. A. Boas, and S. R. Arridge, "Image recon- struction in optical tomography in the presence of coupling errors," Appl. Opt. **46**(14), 2743–2756 (2007).

41. P. K. Yalavarthy, D. R. Lynch, B. W. Pogue, H. Dehghani, and K. D.Paulsen, "Implementation of a computationally efficient least-squares algorithm for highly under-determined three-dimensional diffuse optical tomography problems," Med. Phys. **35(**5), 1682–1697 (2008).

# APPENDICES

## MATLAB PROGRAMING CODES

| | |
|---|---|
| Reconstructing single anomaly in NIRFAST | run_single.m |
| Reconstructing dual anomaly in NIRFAST | run_dual.m |
| Adding a blob to the mesh | add_blob_fl_direct.m |
| Plot the reconstructed or the set mesh | plotmesh_fl.m |
| Conventional reconstruction | reconstruct_fl_dc.m |
| Depth compensation Algorithm | recon_fl_DCA_dc.m |
| Geometric sensitivity Difference Algorithm | recon_fl_GSD_dc.m |

run_single.m

```
clc;clear;close all;
mesh=load_mesh(''); %load the FEM mesh that has been created
save_mesh(mesh,'axial_outward_fluor')
%add an anomaly to the FEM mesh that was loaded onto the platform
blob1.x=;blob1.y=;blob1.z=; % the positions of the anomalies
blob1.r=; %raius of the anomaly
%optical properties of the anomaly
blob1.muax=mesh.muax;blob1.musx=mesh.musx;
blob1.muam=mesh.muam;blob1.musm=mesh.musm;
blob1.muaf=mesh.muaf;blob1.eta=;
blob1.tau=0;
blob1.ri=1.33;blob1.region=1;
mesh_anom = add_blob_fl_direct('axial_outward_fluor',blob1); %add the
anomaly
plotmesh_fl(mesh_anom) %plot the set mesh
save_mesh(mesh_anom,'axial_outward_fluor_with_anomaly')
data_dc_fl = femdata_fl(mesh_anom,0);
data_noise =
add_noise('data_anom_test_fl.paaxfl',1,1,'data_anom_test_fl_noise.paaxf
l');
save_data(data_dc_fl,  '');
clc;clear;close all;
% lambda=100;
% lambda.type='JJt';
fwd_mesh=load_mesh('');
[mesh,pj_error] = recon_geom_dc_fl(fwd_mesh,...
                    [30 30],...
                    0,...
                    'data_anom_test_fl_noise.paaxfl',...
                    100,...
                    100,...
                    '',...
                    0);
mesh_geom = read_solution('',...
             '');
         plotmesh_fl(mesh_geom)
```

run_dual.m

```
clc;clear;close all;
mesh=load_mesh('');
save_mesh(mesh,'')
blob1.x=;blob1.y=;blob1.z=;
blob1.r=;
blob1.muax=mesh.muax;blob1.musx=mesh.musx;
blob1.muam=mesh.muam;blob1.musm=mesh.musm;
blob1.muaf=mesh.muaf;blob1.eta=;
blob1.tau=0;
blob1.ri=1.33;blob1.region=1;
mesh_anom_1 = add_blob_fl_direct('',blob1);
plotmesh(mesh_anom_1)
save_mesh(mesh_anom_1,'')
blob2.x=25;blob2.y=0;blob2.z=0;
blob2.r=5;
blob2.muax=mesh.muax(1);blob2.musx=mesh.musx(1);
blob2.muam=mesh.muam(1);blob2.musm=mesh.musm(1);
blob2.muaf=mesh.muaf(1).*2;blob2.eta=0.2;
blob2.tau=0;
blob2.ri=1.33;blob2.region=2;
mesh_anom = add_blob_fl_direct('',blob2);
save_mesh(mesh_anom,'')
plotmesh_fl(mesh_anom)
data_dc_fl = femdata_fl(mesh_anom,0);
save_data(data_dc_fl,  '.paa');
data_noise =
add_noise('data_anom_test_fl.paaxfl',1,1,'data_anom_test_fl_noise.paaxf
l');
clc;clear;close all;
% lambda=100;
% lambda.type='JJt';
fwd_mesh=load_mesh('');
[mesh,pj_error] = recon_geom_derv_dc_fl(fwd_mesh,...
                    [30 30],...
                    0,...
                    'data_anom_test_fl_noise.paaxfl',...
                    100,...
                    100,...
                    '',...
                    0);
mesh_geom = read_solution('',...
             '');
         plotmesh_fl(mesh_geom)
```

add_blob_fl_direct.m

```
function mesh = add_blob_fl_direct(mesh_nm,blob)

% used by add_blobs
% adds fluorescence blobs.
%
% Part of NIRFAST package
% H Dehghani 2006

mesh=load_mesh(mesh_nm);

p = 1;
% while p ~= 0
%   p = 1;
  if p == 1
    x = blob.x;
    y = blob.y;
    if mesh.dimension == 3
      z = blob.z;
    elseif mesh.dimension == 2
      z = 0;
    end
    r = blob.r;
    dist = distance(mesh.nodes(:,1:3),ones(length(mesh.bndvtx),1),[x y
z]);
    muax = blob.muax;
    musx = blob.musx;
    muam = blob.muam;
    musm = blob.musm;
    ri   = blob.ri;
    muaf = blob.muaf;
    eta = blob.eta;
    tau = blob.tau;
    region = blob.region;
    kappax = 1./(3*(muax+musx));
    kappam = 1./(3*(muam+musm));
    mesh.muax(find(dist<=r)) = muax;
    mesh.musx(find(dist<=r)) = musx;
    mesh.kappax(find(dist<=r)) = kappax;
    mesh.ri(find(dist<=r)) = ri;
    mesh.muam(find(dist<=r)) = muam;
    mesh.musm(find(dist<=r)) = musm;
    mesh.kappam(find(dist<=r)) = kappam;
    mesh.muaf(find(dist<=r)) = muaf;
    mesh.tau(find(dist<=r)) = tau;
    mesh.eta(find(dist<=r)) = eta;
    mesh.region(find(dist<=r)) = region;
    disp(['Number of nodes modified = ' ...
      num2str(length(find(dist<=r)))]);
  end
% end
```

plotmesh_fl.m

```
function plotmesh_fl(mesh)

% plotmesh(mesh)
% where mesh is either structured variable or mesh filename
% Allows fast and easy viewing of mesh property
% Common usage:  plotmesh('circle2000_86') loads mesh
% s davis 03/27/06
%
% Part of NIRFAST package
% H Dehghani 2006

%***************************************
% If not a workspace variable, load mesh
if ischar(mesh)== 1
    mesh = load_mesh(mesh);
end



%***************************************
% Plotting
%***************************************
figure;
set(gca,'FontSize',28)

% STANDARD NIRFAST CASE
if strcmp(mesh.type,'stnd') == 1
  subplot(1,2,1);
  plotim(mesh,mesh.mua);
  title('\mu_a','FontSize',20);
%   caxis([0.0024 0.0028])
  colorbar('horiz');

  subplot(1,2,2);
  plotim(mesh,mesh.mus);
  title('\mu_s''','FontSize',20);
  colorbar('horiz');

elseif strcmp(mesh.type,'fluor') == 1
%   subplot(3,2,1);
%   plotim(mesh,mesh.muax);
%   title('\mu_{ax}','FontSize',10);
%   colorbar;
%
%   subplot(3,2,2);
%   plotim(mesh,mesh.musx);
%   title('\mu_{sx}''','FontSize',10);
%   colorbar;
%
%   subplot(3,2,3);
%   plotim(mesh,mesh.muam);
%   title('\mu_{am}','FontSize',10);
%   colorbar;
%
```

```
%   subplot(3,2,4);
%   plotim(mesh,mesh.musm);
%   title('\mu_{sm}''','FontSize',10);
%   colorbar;
%
%   subplot(3,2,5);
  if isfield(mesh,'etamuaf') == 1
      plotim(mesh,mesh.etamuaf);
  else
      plotim(mesh,mesh.muaf.*mesh.eta);
  end
  title('\eta\mu_{fl}','FontSize',10);
  colorbar;
%
%   subplot(3,2,6);
%   plotim(mesh,mesh.tau);
%   title('\tau','FontSize',10);
%   colorbar;


elseif strcmp(mesh.type,'spec') == 1
  [nc,junk]=size(mesh.chromscattlist);
  n = ceil((nc-2)/2)+1;
  k = 1;
  for i = 1 : nc-2
    subplot(n,2,k);
    plotim(mesh,mesh.conc(:,i));
    t = char(mesh.chromscattlist(i,1));
    title(t,'FontSize',10);
    colorbar;
    k = k + 1;
  end
  subplot(n,2,k+1);
  plotim(mesh,mesh.sa);
  title('Scatter Amplitude','FontSize',10);
  colorbar;
  subplot(n,2,k+2);
  plotim(mesh,mesh.sp);
  title('Scatter Power','FontSize',10);
  colorbar;
end

function plotim(mesh,val)
h = trisurf(mesh.elements,...
        mesh.nodes(:,1),...
        mesh.nodes(:,2),...
        mesh.nodes(:,3),...
        val);
shading interp;
view(2);
axis equal;
axis off;
colormap hot;
```

reconstruct_fl_dc.m

```
function [fwd_mesh,pj_error] = reconstruct_fl_dc(fwd_mesh,...
                                                 recon_basis,...
                                                 frequency,...
                                                 data_fn,...
                                                 iteration,...
                                                 lambda,...
                                                 output_fn,...
                                                 filter_n)


% A subroutine used in the main reconstruction program for
% fluorescence yield.
% reconstruction program for fluorescence meshes
% See documentation for general operating procedures.
%
% Part of NIRFAST package
% H Dehghani 2006


%***********************************************************
% load fine mesh for fwd solve: can input mesh structured variable
% or load from file
if ischar(fwd_mesh)==1
    fwd_mesh = load_mesh(fwd_mesh);
end

etamuaf_sol=[output_fn '_etamuaf.sol'];
% stau_sol=[output_fn '_tau.sol'];

%***********************************************************
% Initiate log file

    fid_log = fopen([output_fn '.log'],'w');
    fprintf(fid_log,'Forward Mesh    = %s\n',fwd_mesh.name);
    if ischar(recon_basis)
        fprintf(fid_log,'Basis           = %s\n',recon_basis);
    else
        fprintf(fid_log,'Basis           = %s\n',num2str(recon_basis));
    end
    fprintf(fid_log,'Frequency       = %f MHz\n',frequency);
    fprintf(fid_log,'Data File       = %s\n',data_fn);
    fprintf(fid_log,'Initial Regularization  = %d\n',lambda);
    fprintf(fid_log,'Filtering         = %d\n',filter_n);
    fprintf(fid_log,'Output Files    = %s',etamuaf_sol);
    % fprintf(fid_log,'Output Files    = %s',tau_sol);
    fprintf(fid_log,'\n');


% get direct excitation field
data_fwd = femdata(fwd_mesh,100);
data_fwd.phi = data_fwd.phix;
```

```
%*********************************************************
% load recon_mesh
if ischar(recon_basis)
  recon_mesh = load_mesh(recon_basis);
  [fwd_mesh.fine2coarse,...
   recon_mesh.coarse2fine] = second_mesh_basis(fwd_mesh,recon_mesh);
elseif isstruct(recon_basis) == 0
  [fwd_mesh.fine2coarse,recon_mesh] =
pixel_basis(recon_basis,fwd_mesh);
elseif isstruct(recon_basis) == 1
    recon_mesh = recon_basis;
end

%*********************************************************
% read data
anom = load_data(data_fn);

% Only reconstructs fluorescence yield!
anom = log(anom(:,3));

%*********************************************************
% initialize projection error
pj_error=[];

%*********************************************************
% modulation frequency
omega = 2*pi*frequency*1e6;
% set fluorescence variables
fwd_mesh.gamma =
(fwd_mesh.eta.*fwd_mesh.muaf)./(1+(omega.*fwd_mesh.tau).^2);

%*********************************************************
% Iterate
for it = 1 : iteration

    % build jacobian
    [Jwholem,datafl] = jacobian_fl(fwd_mesh,frequency,data_fwd);

    % Read reference data
    clear ref;
    ref(:,1) = log(datafl.amplitudem);

    data_diff = (anom-ref);
    pj_error = [pj_error sum((anom-ref).^2)];


    %**********************
    % Screen and Log Info

    disp('---------------------------------');
    disp(['Iteration_fl Number          = ' num2str(it)]);
    disp(['Projection_fl error          = ' num2str(pj_error(end))]);
```

```
    fprintf(fid_log,'---------------------------------\n');
    fprintf(fid_log,'Iteration_fl Number          = %d\n',it);
    fprintf(fid_log,'Projection_fl error = %f\n',pj_error(end));
        if it ~= 1
        p = (pj_error(end-1)-pj_error(end))*100/pj_error(end-1);
        disp(['Projection error change   = ' num2str(p) '%']);
        fprintf(fid_log,'Projection error change   = %f %%\n',p);
        if (p) <= 1
            disp('---------------------------------');
            disp('STOPPING CRITERIA FOR FLUORESCENCE COMPONENT
REACHED');
            fprintf(fid_log,'---------------------------------\n');
            fprintf(fid_log,'STOPPING CRITERIA FOR FLUORESCENCE
COMPONENT REACHED\n');
            % set output
            data_recon.elements = fwd_mesh.elements;
            data_recon.etamuaf = fwd_mesh.etamuaf;
            break
        end
    end
    %************************
    clear data_recon

    % Interpolate Jacobian onto recon mesh
    [Jm,recon_mesh] =
interpolatef2r_fl(fwd_mesh,recon_mesh,Jwholem.completem);
    Jm = Jm(1:2:end-1, 1:end/2); % take only intensity portion

    % Normalize Jacobian wrt fl source gamma
    Jm = Jm*diag([recon_mesh.gamma]);

    % build Hessian
    [nrow,ncol]=size(Jm);
    Hess = zeros(nrow);
    Hess = Jm*Jm';

    % initailize temp Hess, data and mesh, incase PJ increases.
    Hess_tmp = Hess;
    mesh_tmp = recon_mesh;
    data_tmp = data_diff;



    % add regularization
    reg = lambda.*(max(diag(Hess)));
    disp(['Regularization Fluor          = ' num2str(reg)]);
    fprintf(fid_log,'Regularization Fluor           = %f\n',reg);
    Hess = Hess+(eye(nrow).*reg);

    % Calculate update
    u = Jm'*(Hess\data_diff);
    u = u.*[recon_mesh.gamma];

    % value update:
    recon_mesh.gamma = recon_mesh.gamma+u;
```

```
    recon_mesh.etamuaf =
recon_mesh.gamma.*(1+(omega.*recon_mesh.tau).^2);
    % assuming we know eta
    recon_mesh.muaf = recon_mesh.etamuaf./recon_mesh.eta;
    clear u Hess Hess_norm tmp data_diff G

    % interpolate onto fine mesh
    [fwd_mesh,recon_mesh] = interpolatep2f_fl(fwd_mesh,recon_mesh);

    % filter
    if filter_n ~= 0
        disp('Filtering');
        fwd_mesh = mean_filter(fwd_mesh,filter_n);
    end


    %*******************************************************
    % Write solution to file

    if it == 1
        fid = fopen(etamuaf_sol,'w');
    else
        fid = fopen(etamuaf_sol,'a');
    end
    fprintf(fid,'solution %d ',it);
    fprintf(fid,'-size=%g ',length(fwd_mesh.nodes));
    fprintf(fid,'-components=1 ');
    fprintf(fid,'-type=nodal\n');
    fprintf(fid,'%g ',fwd_mesh.etamuaf);
    fprintf(fid,'\n');
    fclose(fid);

end
fin_it = it-1;

%*****************************************************
% Sub functions
function [val_int,recon_mesh] =
interpolatef2r_fl(fwd_mesh,recon_mesh,val)

% This function interpolates fwd_mesh into recon_mesh
% For the Jacobian it is an integration!
NNC = size(recon_mesh.nodes,1);
NNF = size(fwd_mesh.nodes,1);
NROW = size(val,1);
val_int = zeros(NROW,NNC*2);

for i = 1 : NNF
    if recon_mesh.coarse2fine(i,1) ~= 0
        val_int(:,recon_mesh.elements(recon_mesh.coarse2fine(i,1),:)) =
...

val_int(:,recon_mesh.elements(recon_mesh.coarse2fine(i,1),:)) + ...
            val(:,i)*recon_mesh.coarse2fine(i,2:end);
```

```
val_int(:,recon_mesh.elements(recon_mesh.coarse2fine(i,1),:)+NNC) = ...

val_int(:,recon_mesh.elements(recon_mesh.coarse2fine(i,1),:)+NNC) + ...
            val(:,i+NNF)*recon_mesh.coarse2fine(i,2:end);
    elseif recon_mesh.coarse2fine(i,1) == 0
        dist =
distance(fwd_mesh.nodes,fwd_mesh.bndvtx,recon_mesh.nodes(i,:));
        mindist = find(dist==min(dist));
        mindist = mindist(1);
        val_int(:,i) = val(:,mindist);
        val_int(:,i+NNC) = val(:,mindist+NNF);
    end
end

for i = 1 : NNC
    if fwd_mesh.fine2coarse(i,1) ~= 0
        recon_mesh.region(i,1) = ...

median(fwd_mesh.region(fwd_mesh.elements(fwd_mesh.fine2coarse(i,1),:)))
;
        recon_mesh.eta(i,1) = (fwd_mesh.fine2coarse(i,2:end) * ...

fwd_mesh.eta(fwd_mesh.elements(fwd_mesh.fine2coarse(i,1),:)));
        recon_mesh.muaf(i,1) = (fwd_mesh.fine2coarse(i,2:end) * ...

fwd_mesh.muaf(fwd_mesh.elements(fwd_mesh.fine2coarse(i,1),:)));
        recon_mesh.gamma(i,1) = (fwd_mesh.fine2coarse(i,2:end) * ...

fwd_mesh.gamma(fwd_mesh.elements(fwd_mesh.fine2coarse(i,1),:)));
        recon_mesh.tau(i,1) = (fwd_mesh.fine2coarse(i,2:end) * ...

fwd_mesh.tau(fwd_mesh.elements(fwd_mesh.fine2coarse(i,1),:)));

    elseif fwd_mesh.fine2coarse(i,1) == 0
        dist = distance(fwd_mesh.nodes,...
            fwd_mesh.bndvtx,...
            [recon_mesh.nodes(i,1:2) 0]);
        mindist = find(dist==min(dist));
        mindist = mindist(1);
        recon_mesh.region(i,1) = fwd_mesh.region(mindist);
        recon_mesh.eta(i,1) = fwd_mesh.eta(mindist);
        recon_mesh.muaf(i,1) = fwd_mesh.muaf(mindist);
        recon_mesh.gamma(i,1) = fwd_mesh.gamma(mindist);
        recon_mesh.tau(i,1) = fwd_mesh.tau(mindist);

    end
end

function [fwd_mesh,recon_mesh] = interpolatep2f_fl(fwd_mesh,recon_mesh)

for i = 1 : length(fwd_mesh.nodes)
  fwd_mesh.gamma(i,1) = ...
      (recon_mesh.coarse2fine(i,2:end) * ...

recon_mesh.gamma(recon_mesh.elements(recon_mesh.coarse2fine(i,1),:)));
```

```
  fwd_mesh.muaf(i,1) = ...
      (recon_mesh.coarse2fine(i,2:end) * ...

recon_mesh.muaf(recon_mesh.elements(recon_mesh.coarse2fine(i,1),:)));
   fwd_mesh.eta(i,1) = ...
      (recon_mesh.coarse2fine(i,2:end) * ...

recon_mesh.eta(recon_mesh.elements(recon_mesh.coarse2fine(i,1),:)));
  fwd_mesh.etamuaf(i,1) = ...
      (recon_mesh.coarse2fine(i,2:end) * ...

recon_mesh.etamuaf(recon_mesh.elements(recon_mesh.coarse2fine(i,1),:)))
;
  fwd_mesh.tau(i,1) = ...
      (recon_mesh.coarse2fine(i,2:end) * ...

recon_mesh.tau(recon_mesh.elements(recon_mesh.coarse2fine(i,1),:)));
end
```

recon_fl_DCA_dc.m

```
function [fwd_mesh,pj_error] = recon_dca_fl_dc(fwd_mesh,...
                                               recon_basis,...
                                               frequency,...
                                               data_fn,...
                                               iteration,...
                                               lambda,...
                                               output_fn,...
                                               filter_n,...
                                               gap)


% A subroutine used in the main reconstruction program for
% fluorescence yield.
% reconstruction program for fluorescence meshes
% See documentation for general operating procedures.
%
% Part of NIRFAST package
% H Dehghani 2006


%***********************************************************
% load fine mesh for fwd solve: can input mesh structured variable
% or load from file
if ischar(fwd_mesh)==1
    fwd_mesh = load_mesh(fwd_mesh);
end

etamuaf_sol=[output_fn '_etamuaf.sol'];
% stau_sol=[output_fn '_tau.sol'];

%***********************************************************
% Initiate log file
```

```
    fid_log = fopen([output_fn '.log'],'w');
    fprintf(fid_log,'Forward Mesh   = %s\n',fwd_mesh.name);
    if ischar(recon_basis)
        fprintf(fid_log,'Basis          = %s\n',recon_basis);
    else
        fprintf(fid_log,'Basis          = %s\n',num2str(recon_basis));
    end
    fprintf(fid_log,'Frequency      = %f MHz\n',frequency);
    fprintf(fid_log,'Data File      = %s\n',data_fn);
    fprintf(fid_log,'Initial Regularization  = %d\n',lambda);
    fprintf(fid_log,'Filtering        = %d\n',filter_n);
    fprintf(fid_log,'Output Files   = %s',etamuaf_sol);
    % fprintf(fid_log,'Output Files   = %s',tau_sol);
    fprintf(fid_log,'\n');


% get direct excitation field
data_fwd = femdata(fwd_mesh,100);
data_fwd.phi = data_fwd.phix;

%*********************************************************
% load recon_mesh
if ischar(recon_basis)
  recon_mesh = load_mesh(recon_basis);
  [fwd_mesh.fine2coarse,...
   recon_mesh.coarse2fine] = second_mesh_basis(fwd_mesh,recon_mesh);
elseif isstruct(recon_basis) == 0
  [fwd_mesh.fine2coarse,recon_mesh] =
pixel_basis(recon_basis,fwd_mesh);
elseif isstruct(recon_basis) == 1
    recon_mesh = recon_basis;
end
%.........Krishna.....................................
[layer,layer_indx]=cal_dis(recon_mesh,gap);
%*********************************************************
% read data
anom = load_data(data_fn);

% Only reconstructs fluorescence yield!
anom = log(anom(:,3));

%*********************************************************
% initialize projection error
pj_error=[];

%*********************************************************
% modulation frequency
omega = 2*pi*frequency*1e6;
% set fluorescence variables
fwd_mesh.gamma =
(fwd_mesh.eta.*fwd_mesh.muaf)./(1+(omega.*fwd_mesh.tau).^2);

%*********************************************************
% Iterate
```

```
for it = 1 : iteration

    % build jacobian
    [Jwholem,datafl] = jacobian_fl(fwd_mesh,frequency,data_fwd);

    % Read reference data
    clear ref;
    ref(:,1) = log(datafl.amplitudem);

    data_diff = (anom(:,1)-ref(:,1));
    pj_error = [pj_error sum((anom(:,1)-ref(:,1)).^2)];

    %************************
    % Screen and Log Info

    disp('---------------------------------');
    disp(['Iteration_fl Number          = ' num2str(it)]);
    disp(['Projection_fl error          = ' num2str(pj_error(end))]);


    fprintf(fid_log,'---------------------------------\n');
    fprintf(fid_log,'Iteration_fl Number          = %d\n',it);
    fprintf(fid_log,'Projection_fl error          =
%f\n',pj_error(end));

    if it ~= 1
        p = (pj_error(end-1)-pj_error(end))*100/pj_error(end-1);
        disp(['Projection error change   = ' num2str(p) '%']);
        fprintf(fid_log,'Projection error change   = %f %%\n',p);
        if (p) <= 1
            disp('---------------------------------');
            disp('STOPPING CRITERIA FOR FLUORESCENCE COMPONENT
REACHED');
            fprintf(fid_log,'---------------------------------\n');
            fprintf(fid_log,'STOPPING CRITERIA FOR FLUORESCENCE
COMPONENT REACHED\n');
            % set output
            data_recon.elements = fwd_mesh.elements;
            data_recon.etamuaf = fwd_mesh.etamuaf;
            break
        end
    end
    %************************
    clear data_recon

    % Interpolate Jacobian onto recon mesh
    [Jm,recon_mesh] =
interpolatef2r_fl(fwd_mesh,recon_mesh,Jwholem.completem);
    Jm = Jm(1:2:end-1, 1:end/2); % take only intensity portion

    % Normalize Jacobian wrt fl source gamma
    Jm = Jm*diag([recon_mesh.gamma]);
    [nrow,ncol]=size(Jm);
    %.....................DCA-Krishna.................
    layer_size=size(layer,1);
```

```
  dca_reg=zeros(nrow,size(layer,1));
  for ii=1:layer_size
     Jm_sub_tmp=Jm(:,layer{ii,1});
     [U_tmp,S_tmp,V_tmp]=svd(Jm_sub_tmp);
     dca_reg_fl(ii)=max(max(S_tmp,[],1),[],2);

     %J_sub_tmp=J(:,layer{ii,1}+ncol/2);
     %[U_tmp,S_tmp,V_tmp]=svd(J_sub_tmp);
     %dca_reg_mua(ii)  =max(max(S_tmp,[],1),[],2);
  end
  dca_reg_fl_full=[];
  %dca_reg_mua_full=[];
  for ii=1:length(layer_indx)
      for jj=1:size(dca_reg,2)
          if jj==layer_indx(ii)
            dca_reg_fl_full=[dca_reg_fl_full dca_reg_fl(jj)];
            %dca_reg_mua_full  =[dca_reg_mua_full   dca_reg_mua(jj)];
          end
      end
  end
  dca_reg_full=diag([dca_reg_fl_full]);
  Jm=Jm*abs(dca_reg_full.^2);

%.....................................................................
%%
    % build Hessian
    Hess = zeros(nrow);
    Hess = Jm*Jm';

    % initailize temp Hess, data and mesh, incase PJ increases.
    Hess_tmp = Hess;
    mesh_tmp = recon_mesh;
    data_tmp = data_diff;


    % add regularization
    %reg = lambda.*(max(diag(Hess)));
    %disp(['Regularization Fluor           = ' num2str(reg)]);
    %fprintf(fid_log,'Regularization Fluor            = %f\n',reg);
    %Hess = Hess+(eye(nrow).*reg);
    % Add regularization
  if it ~= 1
    lambda = lambda./10^0.25;
  end
% %----nirfast
%  reg_amp = lambda*max(diag(Hess));
%   reg = ones(nrow,1);
%   reg = reg.*reg_amp;
%   Hess = Hess+diag(reg);
%   % Calculate update
%   foo = J'*(Hess\data_diff);
%   foo = foo.*[recon_mesh.kappa;recon_mesh.mua];
% %----nirfast
%----dca
    [U_tmp_Jm,S_tmp_Jm,V_tmp_Jm]=svd(Jm);
    s_max=max(max(S_tmp_Jm,[],1),[],2);
```

```
    reg = lambda*s_max.*eye(size(Hess));
    Hess = Hess+reg;
    u = Jm'*(Hess\data_diff);%dca_reg_full*
    %Hess=foo;
%----dca
    % Calculate update
    %u = Jm'*(Hess\data_diff);
    u = u.*[recon_mesh.gamma];

    % value update:
    recon_mesh.gamma = recon_mesh.gamma+u;
    recon_mesh.etamuaf =
recon_mesh.gamma.*(1+(omega.*recon_mesh.tau).^2);
    % assuming we know eta
    recon_mesh.muaf = recon_mesh.etamuaf./recon_mesh.eta;
    clear u Hess Hess_norm tmp data_diff G

    % interpolate onto fine mesh
    [fwd_mesh,recon_mesh] = interpolatep2f_fl(fwd_mesh,recon_mesh);

    % filter
    if filter_n ~= 0
        disp('Filtering');
        fwd_mesh = mean_filter(fwd_mesh,filter_n);
    end


    %*******************************************************
    % Write solution to file

    if it == 1
        fid = fopen(etamuaf_sol,'w');
    else
        fid = fopen(etamuaf_sol,'a');
    end
    fprintf(fid,'solution %d ',it);
    fprintf(fid,'-size=%g ',length(fwd_mesh.nodes));
    fprintf(fid,'-components=1 ');
    fprintf(fid,'-type=nodal\n');
    fprintf(fid,'%g ',fwd_mesh.etamuaf);
    fprintf(fid,'\n');
    fclose(fid);

end
fin_it = it-1;

%*****************************************************
% Sub functions
function [val_int,recon_mesh] =
interpolatef2r_fl(fwd_mesh,recon_mesh,val)

% This function interpolates fwd_mesh into recon_mesh
% For the Jacobian it is an integration!
NNC = size(recon_mesh.nodes,1);
NNF = size(fwd_mesh.nodes,1);
```

```
NROW = size(val,1);
val_int = zeros(NROW,NNC*2);

for i = 1 : NNF
    if recon_mesh.coarse2fine(i,1) ~= 0
        val_int(:,recon_mesh.elements(recon_mesh.coarse2fine(i,1),:)) =
...

val_int(:,recon_mesh.elements(recon_mesh.coarse2fine(i,1),:)) + ...
            val(:,i)*recon_mesh.coarse2fine(i,2:end);

val_int(:,recon_mesh.elements(recon_mesh.coarse2fine(i,1),:)+NNC) = ...

val_int(:,recon_mesh.elements(recon_mesh.coarse2fine(i,1),:)+NNC) + ...
            val(:,i+NNF)*recon_mesh.coarse2fine(i,2:end);
    elseif recon_mesh.coarse2fine(i,1) == 0
        dist =
distance(fwd_mesh.nodes,fwd_mesh.bndvtx,recon_mesh.nodes(i,:));
        mindist = find(dist==min(dist));
        mindist = mindist(1);
        val_int(:,i) = val(:,mindist);
        val_int(:,i+NNC) = val(:,mindist+NNF);
    end
end

for i = 1 : NNC
    if fwd_mesh.fine2coarse(i,1) ~= 0
        recon_mesh.region(i,1) = ...

median(fwd_mesh.region(fwd_mesh.elements(fwd_mesh.fine2coarse(i,1),:)))
;
        recon_mesh.eta(i,1) = (fwd_mesh.fine2coarse(i,2:end) * ...

fwd_mesh.eta(fwd_mesh.elements(fwd_mesh.fine2coarse(i,1),:)));
        recon_mesh.muaf(i,1) = (fwd_mesh.fine2coarse(i,2:end) * ...

fwd_mesh.muaf(fwd_mesh.elements(fwd_mesh.fine2coarse(i,1),:)));
        recon_mesh.gamma(i,1) = (fwd_mesh.fine2coarse(i,2:end) * ...

fwd_mesh.gamma(fwd_mesh.elements(fwd_mesh.fine2coarse(i,1),:)));
        recon_mesh.tau(i,1) = (fwd_mesh.fine2coarse(i,2:end) * ...

fwd_mesh.tau(fwd_mesh.elements(fwd_mesh.fine2coarse(i,1),:)));

    elseif fwd_mesh.fine2coarse(i,1) == 0
        dist = distance(fwd_mesh.nodes,...
            fwd_mesh.bndvtx,...
            [recon_mesh.nodes(i,1:2) 0]);
        mindist = find(dist==min(dist));
        mindist = mindist(1);
        recon_mesh.region(i,1) = fwd_mesh.region(mindist);
        recon_mesh.eta(i,1) = fwd_mesh.eta(mindist);
        recon_mesh.muaf(i,1) = fwd_mesh.muaf(mindist);
        recon_mesh.gamma(i,1) = fwd_mesh.gamma(mindist);
        recon_mesh.tau(i,1) = fwd_mesh.tau(mindist);
```

```
    end
end

function [fwd_mesh,recon_mesh] = interpolatep2f_fl(fwd_mesh,recon_mesh)

for i = 1 : length(fwd_mesh.nodes)
  fwd_mesh.gamma(i,1) = ...
      (recon_mesh.coarse2fine(i,2:end) * ...

recon_mesh.gamma(recon_mesh.elements(recon_mesh.coarse2fine(i,1),:)));
  fwd_mesh.muaf(i,1) = ...
      (recon_mesh.coarse2fine(i,2:end) * ...

recon_mesh.muaf(recon_mesh.elements(recon_mesh.coarse2fine(i,1),:)));
   fwd_mesh.eta(i,1) = ...
      (recon_mesh.coarse2fine(i,2:end) * ...

recon_mesh.eta(recon_mesh.elements(recon_mesh.coarse2fine(i,1),:)));
  fwd_mesh.etamuaf(i,1) = ...
      (recon_mesh.coarse2fine(i,2:end) * ...

recon_mesh.etamuaf(recon_mesh.elements(recon_mesh.coarse2fine(i,1),:)))
;
  fwd_mesh.tau(i,1) = ...
      (recon_mesh.coarse2fine(i,2:end) * ...

recon_mesh.tau(recon_mesh.elements(recon_mesh.coarse2fine(i,1),:)));
end
```

recon_geom_dc_fl.m

```
function [fwd_mesh,pj_error] = recon_geom_dc_fl(fwd_mesh,...
                                                recon_basis,...
                                                frequency,...
                                                data_fn,...
                                                iteration,...
                                                lambda,...
                                                output_fn,...
                                                filter_n)


% A subroutine used in the main reconstruction program for
% fluorescence yield.
% reconstruction program for fluorescence meshes
% See documentation for general operating procedures.
%
% Part of NIRFAST package
% H Dehghani 2006

%-----------krishna
% always CW for fluor
frequency = 100;
%-----------krishna
```

```
%************************************************************
% load fine mesh for fwd solve: can input mesh structured variable
% or load from file
if ischar(fwd_mesh)==1
    fwd_mesh = load_mesh(fwd_mesh);
end

etamuaf_sol=[output_fn '_etamuaf.sol'];
% stau_sol=[output_fn '_tau.sol'];

%************************************************************
% Initiate log file

    fid_log = fopen([output_fn '.log'],'w');
    fprintf(fid_log,'Forward Mesh   = %s\n',fwd_mesh.name);
    if ischar(recon_basis)
        fprintf(fid_log,'Basis          = %s\n',recon_basis);
    else
        fprintf(fid_log,'Basis          = %s\n',num2str(recon_basis));
    end
    fprintf(fid_log,'Frequency      = %f MHz\n',frequency);
    fprintf(fid_log,'Data File      = %s\n',data_fn);
    fprintf(fid_log,'Initial Regularization  = %d\n',lambda);
    fprintf(fid_log,'Filtering        = %d\n',filter_n);
    fprintf(fid_log,'Output Files   = %s',etamuaf_sol);
    % fprintf(fid_log,'Output Files   = %s',tau_sol);
    fprintf(fid_log,'\n');


% get direct excitation field
data_fwd = femdata(fwd_mesh,100);
data_fwd.phi = data_fwd.phix;

%************************************************************
% load recon_mesh
if ischar(recon_basis)
  recon_mesh = load_mesh(recon_basis);
  [fwd_mesh.fine2coarse,...
   recon_mesh.coarse2fine] = second_mesh_basis(fwd_mesh,recon_mesh);
elseif isstruct(recon_basis) == 0
  [fwd_mesh.fine2coarse,recon_mesh] =
pixel_basis(recon_basis,fwd_mesh);
elseif isstruct(recon_basis) == 1
    recon_mesh = recon_basis;
end

%************************************************************
% read data
anom = load_data(data_fn);

% Only reconstructs fluorescence yield!
anom = log(anom(:,3));

%-change
anom_geom=data_dc_stnd2geom(anom,fwd_mesh);
```

```
%-change

%************************************************************
% initialize projection error
pj_error=[];

%************************************************************
% modulation frequency
omega = 2*pi*frequency*1e6;
% set fluorescence variables
fwd_mesh.gamma =
(fwd_mesh.eta.*fwd_mesh.muaf)./(1+(omega.*fwd_mesh.tau).^2);

%************************************************************
% Iterate
for it = 1 : iteration

    % build jacobian
    [Jwholem,datafl] = jacobian_fl(fwd_mesh,frequency,data_fwd);

    % Read reference data
    clear ref;
    ref(:,1) = log(datafl.amplitudem);
    %-gary
    ref_geom=data_dc_stnd2geom(ref,fwd_mesh);

    data_diff = (anom_geom(:,1)-ref_geom(:,1));
    %-gary
    pj_error = [pj_error sum(data_diff.^2)];


    %***********************
    % Screen and Log Info

    disp('---------------------------------');
    disp(['Iteration_fl Number          = ' num2str(it)]);
    disp(['Projection_fl error          = ' num2str(pj_error(end))]);


    fprintf(fid_log,'---------------------------------\n');
    fprintf(fid_log,'Iteration_fl Number          = %d\n',it);
    fprintf(fid_log,'Projection_fl error          =
%f\n',pj_error(end));

    if it ~= 1
        p = (pj_error(end-1)-pj_error(end))*100/pj_error(end-1);
        disp(['Projection error change   = ' num2str(p) '%']);
        fprintf(fid_log,'Projection error change   = %f %%\n',p);
        if (p) <= 1
            disp('---------------------------------');
            disp('STOPPING CRITERIA FOR FLUORESCENCE COMPONENT
REACHED');
            fprintf(fid_log,'---------------------------------\n');
```

```
            fprintf(fid_log,'STOPPING CRITERIA FOR FLUORESCENCE
COMPONENT REACHED\n');
            % set output
            data_recon.elements = fwd_mesh.elements;
            data_recon.etamuaf = fwd_mesh.etamuaf;
            break
        end
    end
    %************************
    clear data_recon

    % Interpolate Jacobian onto recon mesh
    [Jm,recon_mesh] =
interpolatef2r_fl(fwd_mesh,recon_mesh,Jwholem.completem);
    %-----------------change----------------------%

    Jm = Jm(1:2:end-1, 1:end/2); % take only intensity portion
%     Jm = Jm(:, 1:end/2);

    J_geom_derv_dc_fl=jacob_dc_stnd2geom(Jm,fwd_mesh);
    Jm=J_geom_derv_dc_fl;
    %-----------------change----------------------%

    % Normalize Jacobian wrt fl source gamma
    Jm = Jm*diag([recon_mesh.gamma]);

    % build Hessian
    [nrow,ncol]=size(Jm);
    Hess = zeros(nrow);
    Hess = Jm*Jm';

    % initailize temp Hess, data and mesh, incase PJ increases.
    Hess_tmp = Hess;
    mesh_tmp = recon_mesh;
    data_tmp = data_diff;


    % add regularization
    reg = lambda.*(max(diag(Hess)));
    disp(['Regularization Fluor           = ' num2str(reg)]);
    fprintf(fid_log,'Regularization Fluor           = %f\n',reg);
    Hess = Hess+(eye(nrow).*reg);

    % Calculate update
    u = Jm'*(Hess\data_diff);
    u = u.*[recon_mesh.gamma];

    % value update:
    recon_mesh.gamma = recon_mesh.gamma+u;
    recon_mesh.etamuaf =
recon_mesh.gamma.*(1+(omega.*recon_mesh.tau).^2);
    % assuming we know eta
    recon_mesh.muaf = recon_mesh.etamuaf./recon_mesh.eta;
    clear u Hess Hess_norm tmp data_diff G
```

```
    % interpolate onto fine mesh
    [fwd_mesh,recon_mesh] = interpolatep2f_fl(fwd_mesh,recon_mesh);

    % filter
    if filter_n ~= 0
        disp('Filtering');
        fwd_mesh = mean_filter(fwd_mesh,filter_n);
    end

    %*******************************************************
    % Write solution to file

    if it == 1
        fid = fopen(etamuaf_sol,'w');
    else
        fid = fopen(etamuaf_sol,'a');
    end
    fprintf(fid,'solution %d ',it);
    fprintf(fid,'-size=%g ',length(fwd_mesh.nodes));
    fprintf(fid,'-components=1 ');
    fprintf(fid,'-type=nodal\n');
    fprintf(fid,'%g ',fwd_mesh.etamuaf);
    fprintf(fid,'\n');
    fclose(fid);

end
fin_it = it-1;

%*****************************************************
% Sub functions
function [val_int,recon_mesh] =
interpolatef2r_fl(fwd_mesh,recon_mesh,val)

% This function interpolates fwd_mesh into recon_mesh
% For the Jacobian it is an integration!
NNC = size(recon_mesh.nodes,1);
NNF = size(fwd_mesh.nodes,1);
NROW = size(val,1);
val_int = zeros(NROW,NNC*2);

for i = 1 : NNF
    if recon_mesh.coarse2fine(i,1) ~= 0
        val_int(:,recon_mesh.elements(recon_mesh.coarse2fine(i,1),:)) =
...

val_int(:,recon_mesh.elements(recon_mesh.coarse2fine(i,1),:)) + ...
            val(:,i)*recon_mesh.coarse2fine(i,2:end);

val_int(:,recon_mesh.elements(recon_mesh.coarse2fine(i,1),:)+NNC) = ...

val_int(:,recon_mesh.elements(recon_mesh.coarse2fine(i,1),:)+NNC) + ...
            val(:,i+NNF)*recon_mesh.coarse2fine(i,2:end);
    elseif recon_mesh.coarse2fine(i,1) == 0
        dist =
distance(fwd_mesh.nodes,fwd_mesh.bndvtx,recon_mesh.nodes(i,:));
```

```
        mindist = find(dist==min(dist));
        mindist = mindist(1);
        val_int(:,i) = val(:,mindist);
        val_int(:,i+NNC) = val(:,mindist+NNF);
    end
end

for i = 1 : NNC
    if fwd_mesh.fine2coarse(i,1) ~= 0
        recon_mesh.region(i,1) = ...

median(fwd_mesh.region(fwd_mesh.elements(fwd_mesh.fine2coarse(i,1),:)))
;
        recon_mesh.eta(i,1) = (fwd_mesh.fine2coarse(i,2:end) * ...

fwd_mesh.eta(fwd_mesh.elements(fwd_mesh.fine2coarse(i,1),:)));
        recon_mesh.muaf(i,1) = (fwd_mesh.fine2coarse(i,2:end) * ...

fwd_mesh.muaf(fwd_mesh.elements(fwd_mesh.fine2coarse(i,1),:)));
        recon_mesh.gamma(i,1) = (fwd_mesh.fine2coarse(i,2:end) * ...

fwd_mesh.gamma(fwd_mesh.elements(fwd_mesh.fine2coarse(i,1),:)));
        recon_mesh.tau(i,1) = (fwd_mesh.fine2coarse(i,2:end) * ...

fwd_mesh.tau(fwd_mesh.elements(fwd_mesh.fine2coarse(i,1),:)));

    elseif fwd_mesh.fine2coarse(i,1) == 0
        dist = distance(fwd_mesh.nodes,...
            fwd_mesh.bndvtx,...
            [recon_mesh.nodes(i,1:2) 0]);
        mindist = find(dist==min(dist));
        mindist = mindist(1);
        recon_mesh.region(i,1) = fwd_mesh.region(mindist);
        recon_mesh.eta(i,1) = fwd_mesh.eta(mindist);
        recon_mesh.muaf(i,1) = fwd_mesh.muaf(mindist);
        recon_mesh.gamma(i,1) = fwd_mesh.gamma(mindist);
        recon_mesh.tau(i,1) = fwd_mesh.tau(mindist);

    end
end

function [fwd_mesh,recon_mesh] = interpolatep2f_fl(fwd_mesh,recon_mesh)

for i = 1 : length(fwd_mesh.nodes)
  fwd_mesh.gamma(i,1) = ...
      (recon_mesh.coarse2fine(i,2:end) * ...

recon_mesh.gamma(recon_mesh.elements(recon_mesh.coarse2fine(i,1),:)));
  fwd_mesh.muaf(i,1) = ...
      (recon_mesh.coarse2fine(i,2:end) * ...

recon_mesh.muaf(recon_mesh.elements(recon_mesh.coarse2fine(i,1),:)));
   fwd_mesh.eta(i,1) = ...
      (recon_mesh.coarse2fine(i,2:end) * ...

recon_mesh.eta(recon_mesh.elements(recon_mesh.coarse2fine(i,1),:)));
```

```
  fwd_mesh.etamuaf(i,1) = ...
      (recon_mesh.coarse2fine(i,2:end) * ...

recon_mesh.etamuaf(recon_mesh.elements(recon_mesh.coarse2fine(i,1),:)))
;
  fwd_mesh.tau(i,1) = ...
      (recon_mesh.coarse2fine(i,2:end) * ...

recon_mesh.tau(recon_mesh.elements(recon_mesh.coarse2fine(i,1),:)));
end
```

VITA

Krishna Teja Tokala

Candidate for the Degree of

Master of Science

Thesis: A GEOMETRIC-SENSITIVITY-DIFFERENCE ALGORITHM FOR FLUORESCENCE DIFFUSED OPTICAL TOMOGRAPHY RECONSTRUCTION.

Major Field: ELECTRICAL ENGINEERING

Biographical:

Education:

Completed the requirements for the Master of Science in ELECTRICAL ENGINEERING at Oklahoma State University, Stillwater, Oklahoma in December, 2013.

Completed the requirements for the Bachelor of Science in ELECTRONICS AND COMMUNICATION ENGINEERING at VELLORE INSTITUTE OF TECHNOLOGY, Vellore, Tamil Nadu/India in 2012.